AAPG BULLETIN

Porosity evolution and geometry in Santos Basin Aptian pre-salt petrofacies

William Freitas, Thisiane Dos Santos, Mariane Trombetta, Sabrina Danni Altenhofen, Argos Belmonte Silveira Schrank, Guilherme Martinez, Anderson Maraschin, Felipe Dalla Vecchia, Amanda Goulart Rodrigues, Luiz Fernando De Ros, and Rosalia Barili

AAPG Bulletin published online 15 November 2025
doi: 10.1306/11132524122

Disclaimer: The AAPG Bulletin Ahead of Print program provides readers with the earliest possible access to articles that have been peer-reviewed and accepted for publication. These articles have not been copyedited and are posted "as is," and do not reflect AAPG editorial changes. Once the accepted manuscript appears in the Ahead of Print area, it will be prepared for print and online publication, which includes copyediting, typesetting, proofreading, and author review. ***This process will likely lead to differences between the accepted manuscript and the final, printed version.*** Manuscripts will remain in the Ahead of Print area until the final, typeset articles are printed. Supplemental material intended, and accepted, for publication is not posted until publication of the final, typeset article.

Cite as: Freitas, W., T. Dos Santos, M. Trombetta, S. D. Altenhofen, A. B. S. Schrank, et al., **Porosity evolution and geometry in Santos Basin Aptian pre-salt petrofacies**, *(in press; preliminary version published online Ahead of Print* 15 November 2025*):* AAPG Bulletin, doi: 10.1306/11132524122.

Copyright © Preliminary Ahead of Print version 2025 by The American Association of Petroleum Geologists

POROSITY EVOLUTION AND GEOMETRY IN SANTOS BASIN APTIAN PRE-SALT PETROFACIES

William Freitas [1,2]; Thisiane Dos Santos[2]; Mariane Trombetta[2]; Sabrina Danni Altenhofen[2]; Argos Belmonte Silveira Schrank[1,2]; Guilherme Martinez[2]; Anderson Maraschin[2]; Felipe Dalla Vecchia[2]; Amanda Goulart Rodrigues[1]; Luiz Fernando De Ros[1] and Rosalia Barili[1,2]

1 Instituto de Geociências, Campus do Vale. Federal University of Rio Grande do Sul (UFRGS), Av. Bento Gonçalves, 9500 Agronomia, Porto Alegre 90650-001, Brazil
goulart.rodrigues@ufrgs.br (A.G.R.); lfderos@inf.ufrgs.br (L.F.D.R.)

2 Institute of Petroleum and Natural Resources (IPR), Building 96J, Pontifical Catholic University of Rio Grande do Sul (PUCRS), Av. Ipiranga, 6681-Partenon, Porto Alegre 90619-900, Brazil;
william.freitas@pucrs.br (W.S.F); thisiane.santos@pucrs.br (T.D.S.); mariane.trombetta@pucrs.br (M.C.T); sabrina.altenhofen@pucrs.br (S.D.A.); argos.schrank@pucrs.br (A.B.S.); guilherme.martinez@pucrs.br (G.M); anderson.maraschin@pucrs.br (A.M.); felipe.vecchia@pucrs.br (F.D.V.); rosalia.cunha@pucrs.br (R.B.)

ABSTRACT

The pre-salt deposits from offshore southeastern Brazil account approximately 3/4 of the total hydrocarbon production of the country. Consequently, they are the subject of various studies aimed at better understanding the primary and diagenetic controls on their reservoir quality. The Barra Velha Formation (Aptian, Santos Basin) constitutes the main reservoirs of the pre-salt sag section, essentially composed of magnesian clays, calcite spherulites and fascicular shrubs, and intraclasts reworked from these aggregates. The pore systems of these rocks are highly complex, owing to depositional and diagenetic controls. Therefore, the origin and distribution of porosity and permeability are difficult to understand. In order to better understand and characterize the pore systems of the unusual pre-salt reservoirs, this study aimed to recognize the relationships among their porosity and permeability values, and pore types, within the context of the evolution and geometry of their pore systems. X-ray microtomography (m-CT) scanning of 251 samples from 3 wells was performed to obtain the three-dimensional (3-D) porosity distribution, and the main pore types were described in detail in 583 thin sections. Thirteen petrofacies were defined for the studied samples, and the 3-D pore network was reconstructed for characteristic samples of each petrofacies. Image segmentation was applied to quantify pore sizes and shapes, as well as to visualize the connections between them. Petrofacies with low quality or considered non-reservoirs correspond to rocks where the magnesian clay matrix was partially replaced by dolomite, or where dolomite or silica filled interparticle pores where pores were generated by matrix dissolution, leading to poorly connected vuggy pores. On the other hand, high quality reservoirs correspond either to in situ rocks with porosity generation mainly through widespread dissolution of the Mg-clay matrix, further enhanced by the dissolution of calcite spherulites and shrubs, as well as reworked rocks with high interparticle primary porosity, and crystalline rocks formed by pervasive dolomite replacement followed by dissolution, creating intercrystalline porosity. Dissolution played not only a significant role in increasing porosity, but also in increasing pore connectivity and pore size, as observed through pore network segmentation tools and through the Area 3D, EqDiameter, and ShapeVA3d attributes. Increased understanding of the pre-salt reservoir porosity patterns is important not only for exploration for new accumulations, but also for optimizing the recovery from currently producing reservoirs.

INTRODUCTION

Most of the pre-salt hydrocarbon reserves are contained in the Barra Velha Formation (BVF), corresponding to the Santos Basin Aptian sag section (ANP, 2025). These rocks represent a unique combination of calcite aggregates, magnesian phyllosilicates, dolomite, and silica (Schrank et al., 2024). The controls of primary and diagenetic characteristics on the quality of these reservoirs are still poorly understood.

The petrographic characterization of the main sag reservoirs revealed that they are composed of divergent fibrous aggregates with a fascicular-optical fabric, characteristic of abiotic chemical precipitation of carbonates in various environments, such as some travertines (Pentecost, 1990; Chafetz and Guidry, 1999; Fouke et al., 2000; Aguillar et al., 2024), Precambrian stromatolites (Grotzinger and Knoll, 1999; Riding, 2008) and lakes (Jones and Renaut, 1994; Warren, 2006: Della Porta, 2015). Another interesting aspect of the pre-salt system corresponds to the voluminous and recurrent deposition of magnesian silicates, such as stevensite and kerolite (Carramal et al., 2022; Silva et al., 2022; Schrank et al., 2024). These clays were commonly replaced and locally encrusted by spherulitic and fascicular calcite aggregates, as well as replaced by dolomite and silica, or dissolved, giving rise to spherulitic reservoirs with secondary porosity (Herlinger et al., 2017; Wright and Barnett, 2017; 2020; Lima and De Ros, 2019). Some characteristics of the Aptian pre-salt deposits can be essentially understood as a product of recurrent, high-frequency, and alternating precipitation of calcite and magnesian silicates. Another very common feature of the pre-salt is the occurrence of intense dissolution, dolomitization, and silicification in the vicinity of major faults and other structures, which can be characterized as hydrothermal alterations (Vieira de Luca et al., 2017; Lima et al., 2020; Wennberg et al., 2021; Strugale et al., 2024).

One of the main challenges in evaluating carbonate reservoirs is understanding the relationship between pore type, porosity and permeability (Lønøy, 2006). Carbonate rocks commonly contain a variety of pore types that can vary in size over several orders of magnitude (Weger et al., 2009). The pore systems of carbonate rocks are complex, and reservoirs typically contain various pore types, of both primary and secondary origin (Mazzullo and Chilingarian, 1992; Worden et al., 2018). On the other hand, understanding the pore systems of the pre-salt reservoirs represents additional challenges. This, because the knowledge of the primary processes and controls on porosity is still incomplete, as is also the understanding of the impact of diagenesis on reservoir quality. Existing classifications of carbonate pore types and pore systems can be partially adapted to the pre-salt reservoirs, but the genetic, geometric, and petrophysical aspects of the pre-salt porosity, and the influence of diagenesis on the pore systems are poorly understood.

Digital rock technology is another approach for studying the petrophysical properties of complex reservoirs, such as those with fractures, complex wettability, or high clay content (Wang et al., 2022). There is a growing body of work trying to apply digital rock or machine learning methods to the pre-salt carbonates and possible analogues (Rezende et al., 2013; Hosa et al., 2020; Rodrigues-Berriguete et al., 2022; Basso et al., 2022; Matheus et al., 2023), however in most cases ignoring the complex and unusual characteristics of the pre-salt rocks. Consequently, most of these proposals have generated models that are quite unrealistic in relation to the geological and petrologic aspects of the pre-salt reservoirs.

The main objective of this study is to characterize the geometry of the pore systems of the Barra Velha Formation pre-salt reservoirs, and the controls exerted on them by the primary and diagenetic aspects during their evolution. To do this, we employ a combination of quantitative petrography, high-resolution three-dimensional images obtained through X-ray microtomography, and conventional petrophysical analysis (porosity and permeability) in selected petrofacies to understand the main controls impacting reservoir quality. Understanding the genesis, evolution, and geometry of porosity in these reservoirs will contribute to optimizing their production efficiency in the Santos Basin, as well as exploration for similar reservoirs.

GEOLOGICAL SETTING

Santos Basin (Fig. 1), located in southeastern Brazilian continental margin, is the widest of the peri-Atlantic basins, bordered to the North with the Campos Basin through the Cabo Frio High, and to the South with the Pelotas Basin through the Florianópolis High. It is the largest offshore basin in the country, covering approximately 350,000 km^2 (Moreira et al., 2007). The basin was formed through the breakup of the Gondwana supercontinent and creation of the South Atlantic Ocean during the Early Cretaceous (Lentini et al., 2010; Blaich et al., 2011; Chaboureau et al., 2013; Freitas et al., 2019; Baptista et al., 2023). The crystalline basement of Santos Basin is constituted by Precambrian granites and gneisses of the Coastal Complex and meta-sediments of the Ribeira Belt (Moreira et al., 2007; Mohriak et al., 2012).

The initial exploration of the basin occurred in the 1970s. Pereira and Feijó (1994) developed the first chronostratigraphic model for the depositional sequences of the basin. The study conducted by (Moreira et al. 2007) refined that previous model, with better distinction of the depositional sequences. Mohriak (2003) interpreted different extensional phases in the evolution of the basin. The onset of extension was associated with asthenospheric uplift and lithospheric thinning. Subsequent phases encompassed lithospheric stretching during rifting, characterized by the extrusion of basaltic lavas and establishment of rift hemi-graben systems filled with lacustrine sediments during the Neocomian-Barremian. At the end of rifting, an episode of lithospheric stretching and uplifting enabled the reactivation of faults and the formation of a vast regional unconformity, the Pre-Alagoas unconformity (Kumar and Gamboa, 1979).

This tectonic evolution resulted in the formation of relatively small lakes during the rift phase, followed by regional uplift, erosion, and thermal subsidence, promoting the creation of a very large lake during the sag phase. The basin was then filled with Aptian lacustrine sediments (Mohriak, 2003). The Florianópolis High blocked the inflow of marine waters from the South. After marine waters could finally enter the large depression, thick and extensive salt layers covered the lacustrine sediments at the end of the Aptian (Farias et al., 2019).

Moreira et al. (2007) divided the basin fill into three depositional supersequences: rift, sag, and drift. The first is composed of the Guaratiba Group, which includes the Camboriú, Piçarras, and Itapema Formations. The Camboriú Formation consists of tholeiitic basalts, representing the economic basement of the basin (Moreira et al., 2007; Mohriak, 2012). The Piçarras Formation comprises alluvial fan polymictic conglomerates and sandstones composed of basalt, quartz, and feldspar fragments in proximal portions, and sandstones, siltstones, and mudstones rich in magnesian clays in the lacustrine portions (Moreira et al., 2007). The Itapema Formation consists of proximal alluvial sandstones and conglomerates, bivalve bioclast calcirudites and calcarenites (“coquinas”), and distal carbonates intercalated with organic dark mudstones that are the main source rocks of the basin (Moreira et al., 2007)

The contact with the sag supersequence is defined by the Pre-Alagoas regional unconformity (Fig. 2; Moreira et al., 2007). Deposition of the Barra Velha Formation occurred in an alkaline lacustrine environment with high rates of evaporation, promoting the formation of calcite spherulites within a matrix of magnesium silicates, and crusts composed of fascicular calcite shrubs. Initially, these deposits were interpreted as microbial (Terra et al., 2010). However, they were reinterpreted as product of abiotic precipitation in an alkaline system (Wright and Barnett, 2015; 2020; Carramal et al., 2022; Wright, 2022; Schrank et al., 2024). The Ariri Formation corresponds to Aptian evaporites, product of repeated marine incursions and desiccations, under arid climate (Moreira et al., 2007).

The Drift supersequence encompasses the Camburi, Frade, and Itamambuca Groups (Moreira *et al*., 2007; Wright and Barnett, 2015). The Camburi Group comprises siliciclastic alluvial fan deposits, shallow platform carbonates, and distal shales deposited during the Albian, as well as proximal alluvial fan deposits, distal shales, and marls associated with turbidites (Moreira *et al*., 2007). The Frade Group consists of alluvial fan deposits from the Santos Formation, fluvial sandstones from the Juréia Formation, and shales and mudstones from the Itajaí-Açu Formation (Moreira *et al*., 2007). The Itamabuca Group comprises fluvial sandstones from the Ponta Aguda Formation, calcarenites and calcirudites from the Iguapé Formation, and finally, the Marambaia Formation composed of shales, mudstones, marls, and diamictites (Moreira *et al*., 2007).

DEPOSITIONAL ENVIRONMENT

The in situ rocks of the Barra Velha Formation were deposited in an extensive meromictic lacustrine system, characterized by a water column stratified into oxygenated (mixolimnion) and anoxic (monimolimnion) layers, separated by a chemocline (De Ros, 2018). This stratification controlled mineral precipitation, favors calcite formation in the upper levels and magnesium clays with spherulites in the lower levels. Rapid variations in the depth of the chemocline influenced the observed lithological changes (Carvalho et al., 2022). This depositional model explains the abrupt alternation between porous and non-porous facies without requiring frequent lake-level fluctuations. The lack of subaerial exposure markers and the isotopic homogeneity between basins support the interpretation of a chemically and structurally stable lacustrine system, which is key for understanding and exploring pre-salt reservoirs.

The reworked deposits of the Barra Velha Formation are composed of intraclasts derived from in situ spherulitic and fascicular deposits, re-cemented by fascicular calcite and interbedded on a millimeter to centimeter scale (Carvalho and Fernandes, 2021; Altenhofen et al., 2024). Their wide distribution, good grain-size sorting, and rounded morphology indicate they do not follow a purely gravitational model (Saller et al., 2016; Camargo et al., 2022). The absence of traction structures suggests that internal waves, triggered by disturbances in the chemocline of stratified lakes, were responsible for reworking processes, promoting episodic erosion and redistribution (Rodríguez-Berriguete et al., 2022; Altenhofen et al., 2024). Multiple reworking cycles, associated with ooids having intraclasts as nuclei, indicate frequent hydrodynamic disturbances in a stable lacustrine system, controlled by internal oscillations of the water column (Carramal et al., 2022; Gomes et al., 2020; Wright, 2022).

MATERIALS AND METHODS

The methodology of this work followed the workflow shown in Figure 3, comprising different analyses that were integrated for interpreting the pore systems of the characteristic Barra Velha petrofacies and their controls. The entire study was based on analyses conducted on three wells located in the Santos Basin. The production data from the wells in field B are confidential. In contrast, well C1 belongs to one of the most prolific pre-salt fields in Brazil, reaching a production of 47,347 bbl/d of oil and 1.374 Mm³/d of natural gas (ANP, 2025).

Core Description

A total of 48.4 m of cores were described from well B1, and 70.6 m from well C1, at 1:20 scale. Facies were classified according to De Ros and Oliveira (2023). Well B2 cores were not available for description.

The lithostratigraphic logs were elaborated in digital format using the Adobe Illustrator software. Core analyses and descriptions were integrated with porosity and permeability data, in order to visualize the distribution of facies and petrophysical data. Facies analysis allowed understanding the heterogeneities of the studied wells and the formation of the studied sag phase pre-salt deposits of the Santos Basin.

Petrography

A total of 583 thin sections (267 from well B1, 120 from well B2 and 197 from well C1) from the selected wells were described using the Petroledge® software (De Ros et al., 2007), a system to assist in the acquisition, processing, and sharing of generated

inary

petrographic data. Petrographic quantification was performed by counting 300 points per thin section, and through visual estimation and comparative tables. All thin sections were prepared from samples impregnated with blue epoxy resin to highlight the porosity. Staining with a solution of alizarin and potassium ferrocyanide allowed identification of the carbonate species (Dickinson, 1966).

The descriptions were performed on ZEISS AXIO A1M and Leica DM750P transmitted light microscopes, with crossed and uncrossed polarizers. Photomicrographic documentation was obtained using ZEN 3.1 Blue Edition and LAS X 5.0.2 software, utilizing AxioCam ICc 3 Flexacam C1 and C3 cameras attached to the microscopes. The system of De Ros and Oliveira (2023) was used for classification of petrofacies of the *in situ* and redeposited rocks.

X-Ray Microtomography

Computerized microtomography analysis was conducted in three stages: (1) image acquisition; (2) reconstruction of micro-CT sections, aimed at processing the images and making corrections to construct the 3D volume; and, (3) calculation of the total or partial volume of the scanned samples. The micro-CT images were captured using SkyScan 1173 equipment, which utilizes a microfocus x-ray source operating at 130kV and 61μA. Pixel sizes ranged from 7μm to 35.7μm and were analyzed using brass filters of 0.25mm to mitigate beam hardening effects. The acquisition process involved a 270- or 360- degree rotation of the object, with a fixed rotation step of 0.2 degrees. At each angular position, a transmission image was captured and stored as 16-bit TIFF files on the hard disk. Following acquisition, reconstruction was performed utilizing a 3-D cone beam algorithm, which accounted for the objects thickness. Once reconstruction was complete, a 3-D image was generated. The AVIZO Thermo Scientific software was used for segmentation, individualization of pores, pore size and pore shape analyses.

Petrophysics

Conventional petrophysical data from three wells were evaluated in this study. Part of the porosity and permeability data were obtained from the National Petroleum Agency (ANP), and another part was analyzed using the AP-608 Porosimeter-Permeameter at the Petroleum and Natural Resources Institute of Pontifical Catholic University of Rio Grande do Sul. The tested samples were plugs of 1 and 1.5 inches in diameter and 1 inch in length. In total, the petrophysical porosity and permeability from 149 samples from well B1, 88 samples from well B2, and 64 samples from well C1 were evaluated and integrated with other results, to assess the key factors controlling the reservoir quality of the rocks.

RESULTS

Cores description

Lithologic description of the cores allowed the identification of six in situ facies (Fig. 4) and three redeposited facies (Fig. 5). The two cores exhibit distinct characteristics and demonstrate significant heterogeneity (Fig. 6). Core B1 is characterized by a dominance of in situ rocks at its base and top, with reworked deposits predominating in the intermediate part. There is limited silicification at the top of the core. The in situ interval at the base is 16.13 m thick and contains high-frequency intercalations of various in situ facies. The reworked deposits have a maximum thickness of 8.7 meters, mainly

preview

comprising calcarenites and rudaceous calcarenites, with thicknesses reaching up to 4.53 and 3.2 meters, respectively.

Core C1 exhibits a dominance of reworked deposits, with significant *in situ* deposits intercalated at the top. In the intermediate portion, there is a predominance of *in situ* rocks, with limited reworked deposits among them. At the base of the core, *in situ* rocks occur, with subordinate reworked deposits. The in situ rocks form a 17.45 m thick package, predominantly composed of shrub-spherulstones and shrubstones. The reworked deposits are up to 2.18m thick, mostly represented by calcarenites and rudaceous calcarenites.

Primary Composition and Texture

The in situ rocks exhibit a diversity of textures and structures (Table 1). Muddy spherulstones often display irregular lamination due to the distribution, concentration, and coalescence of spherulites (Fig. 7A). Shrub-spherulstones exhibit irregular lamination due to the alternation of levels with predominance of spherulites or shrubs (Fig. 7B). Mudstones show both planar-parallel and irregular lamination (Fig. 7C). Reworked samples generally appear with a massive structure (Fig. 7D).

In well B1 core, the in situ samples display laminations characterized by the distribution of spherulites, shrubs, and clay peloids within the Mg-silicate matrix. Calcite spherulites and shrubs replaced the original Mg-silicate matrix and usually engulfing peloids (Schrank et al., 2024). The spherulites have a radius of 0.2 mm to 0.6 mm, while the shrubs are generally larger than 1 mm. The matrix of magnesian phyllosilicates (Carramal et al., 2022; Schrank et al., 2024) is common in this core, and is usually partially or completely replaced by blocky and saddle dolomite, microcrystalline quartz cryptocrystalline silica, and microcrystalline calcite, or simply dissolved. Silt and fine sand siliciclastic grains of feldspars, quartz, micas, rutile, tourmaline and zircon occur locally mixed in the matrix.

In well B2 core, the phyllosilicate matrix of the in situ samples was generally replaced by blocky dolomite, microcrystalline quartz, cryptocrystalline silica, and microcrystalline calcite. Calcite is the most common component in the analyzed samples, mainly found as spherulitic and fascicular aggregates of millimeter to centimeter size. These aggregates are often recrystallized into micro to macrocrystalline anhedral mosaics or as triangular sectors following the original crystal orientation.

In well C1 core, in situ rocks are less common than in the other two wells. Calcite is the most important component in these samples; it occurs in the form of spherulitic, fascicular, and microcrystalline carbonate intraclasts, carbonate intraclasts, shrub and spherulite, and clay ooid generated over a carbonate intraclast. Blocky dolomite, cryptocrystalline, fibrous-radiated chalcedony, and coarsely-crystalline quartz occur replacing matrix, followed by framework-replacive and filling interstitial space.

Diagenetic Processes and Products

The main diagenetic constituents in the analyzed samples are calcite, dolomite, and silica. Other diagenetic phases in smaller quantities include sphalerite, anhydrite, barite, dawsonite, bitumen, and pyrite (Table 2).

The main diagenetic processes that impacted the petrophysical properties of the studied rocks were: dissolution, cementation, replacement and compaction (Fig. 8).

Dissolution

Dissolution played a significant role as the primary process of porosity generation in these rocks. Matrix dissolution porosity is generally abundant, although in many cases only perceptible from replacive dolomite crystals that appear to ‘float’ within the pores formed by dissolution. Partially, pores among the calcite aggregates were also generated by the dissolution of Mg-clay peloids. The shrinkage and partial or complete dissolution of the syngenetic Mg-silicate matrix correspond to the main origin of the porosity present in the analyzed rocks. Matrix dissolution also significantly contributed to permeability, especially where the generated pores were not filled with dolomite, silica or calcite cement.

Additionally, the partial or complete dissolution of shrubs, spherulites, intraclastic particles, and secondary constituents, resulted in intra-aggregate and intraparticle porosity, contributing considerably to total porosity values. However, this process did not contribute to increasing permeability, because these pores are poorly connected.

Preview

Cementation and replacement

Besides forming the characteristic spherulites and shrubs, diagenetic calcite occurs in the form of blocky crystals that replaced the matrix, partially filled the pores formed by its dissolution in the in situ rocks, and interparticle pores in redeposited rocks, as well as vugular pores. Blocky crystals also locally rim the aggregates and intraclasts. Both blocky and macrocrystalline calcite filled pores in the in situ and reworked samples. Microcrystalline calcite replaced clay peloids, intraclasts, and matrix, and also the rare microbial deposits. On the other hand, macrocrystalline calcite commonly filled pores from dissolution of matrix, intraclasts, and peloids, as well as fractures, vugular and interparticle pores.

Dolomite is found in both in situ and reworked rocks, most commonly as euhedral rhombs, often replacing the matrix, calcite aggregates, or particles; but it also acted as cement, filling or rimming the pores. Microcrystalline dolomite also replaced the matrix, calcite aggregates, or particles, and rimmed the carbonate particles. Additionally, dolomite formed lamellar aggregates filling matrix contraction pores and replacing the syngenetic matrix. In some areas, dolomite pseudomorphically replaced the spherulites and shrubs. Saddle dolomite replaced the matrix, aggregates, peloids and intraclasts, with characteristic wavy extinction and defective shapes. It also filled intra-aggregate and intraparticle dissolution pores, as well as channel and vug pores. Macrocrystalline dolomite is mostly found as cement, filling fractures, channels and replacing the matrix.

Microcrystalline quartz commonly replaced components such as carbonate aggregates, intraclasts, Mg-silicate matrix, peloids, and ostracod bioclasts, while macrocrystalline quartz partially filled pores, especially fractures and dissolution pores in calcite aggregates. Both micro and macrocrystalline quartz filled interparticle, inter-aggregate, vugular, channel, and fracture pores, also replacing intraclasts, spherulites, and Mg-silicate matrix. Prismatic quartz is generally found as isolated crystals in inter- and intra-aggregate pores. Fibro-radiated chalcedony is frequently observed in strongly silicified rocks replacing the matrix and spherulites, and also filling matrix dissolution and vugular pores. Microcrystalline quartz and cryptocrystalline silica often replaced carbonate intraclasts and aggregates, as well as peloids and Mg-clay matrix in strongly altered samples. Prismatic quartz filled fracture pores in aggregates and intraclasts, channel, vugular, interparticle, and inter-aggregate pores, as well as pores from dissolution of aggregates and intraclasts. Drusiform quartz typically filled large vugular matrix dissolution and fractures, while prismatic quartz rimmed intra-aggregate, vugular, channel, and fracture pores.

Porosity

The pore types were classified according to the Choquette and Pray (1970) system, with some adaptation for the studied sag phase rocks of the Barra Velha Formation (Fig. 9). The results are presented in Tables 3 and 4.

Porosity of the* in situ *Deposits

In the in situ samples from wells B1, B2, and C1, inter-aggregate pores are the most prevalent types, which can correspond either to primary porosity, in some shrubstones, or to secondary result of matrix dissolution. The occurrence of intra-aggregate dissolution pores, formed either cutting through, or following the internal crystalline fabric, is also common. Intra-aggregate dissolution pores were also formed due to the dissolution of engulfed peloids. Despite being quite common, intra-aggregate pores do not contribute to effective porosity and permeability, because they are poorly connected. Vugular pores are quite common and are often found completely cemented in substantially altered rocks. Where these pores are not obstructed, they play a crucial role in increasing sample permeability. Fractures and channel pores are less frequent, but where volumetrically significant contribute to high permeabilities, akin to the vugular pores.

Porosity of the Redeposited Deposits

The most common type of porosity in the reworked samples corresponds to intraparticle pores resulting from the dissolution of intraclasts, followed by interparticle pores, interpreted as essentially primary depositional, but also subordinately from the dissolution of the clay matrix or of dolomite cement. Particle fracture pores may significantly increase local permeability. Intracrystalline and intercrystalline pores are particularly important in some strongly silicified and dolomitized rocks. Other locally significant pore types in these lithotypes include fractures, channel, and vugular pores, where not partially or completely cemented.

Permeability

Petrophysical porosity and permeability values were plotted for the three studied wells (Fig.10). In the three wells, permeability shows a wide range, from very low permeability to very high values, which is due to the depositional and diagenetic heterogeneity characteristic of the pre-salt reservoirs.

There are significant differences in permeability among the three studied cores. In well B1, the best permeabilities are found in the in situ rocks. Shrubstones show values of up to 1923 md in this well, and it is the class with the best permeability values relative to the porosity. Shrub-spherulstones also show good permeability values, reaching up to 962 md. Among the reworked rocks of well B1, the class with the best permeability are the rudaceous calcarenites, with up to 861.32 md.

The same is observed in well B2 core, where the in situ rocks represent the best permeability values, along with some of the redeposited rocks. The best classes in terms of permeability are shrubstones, shrub-spherulstones and rudaceous calcarenites, with maximum values of 1530 md, 2980 md, and 812 md, respectively.

In well C1, there is a predominance of reworked rocks, and thus the best permeability values are found among them. Arenaceous calcirudites, slightly rudaceous calcarenites, and rudaceous calcarenites are the classes with the best permeability values, with maximum values of 1166.7 md, 716.08 md, and 954.83 md, respectively.

DISCUSSION

Reservoir Petrofacies

The present study applied the reservoir petrofacies concept (sensu De Ros and Goldberg, 2007), as an approach to assess the influence of diagenetic, depositional textural and compositional factors on the reservoir quality of the Barra Velha Formation rocks.

Reservoir petrofacies are characterized by the complex interaction among predominant depositional structures, textures and primary composition, and diagenetic processes controlling porosity. In this study, 13 representative reservoir petrofacies were defined for the BVF samples.

The initial petrofacies definition involved their classification (sensu De Ros and Oliveira, 2023). Specific parameters were then applied to each class. Each petrofacies is identified by a mnemonic code that is related to the classification and the main porosity modifier. For example, "IntracSil" refers to petrofacies formed by intraclastic rocks with high silica content filling interparticle and non-fabric selective pores. For the in situ rocks, nine petrofacies are defined: MudShrPor, MudShrDolPor, MudSpheDol, MudSphePor, MudSpheMtx, Mudstone, ShrPor, ShrSil and ShrDolPor. The defining criteria encompass the following attributes: (1) textural: the framework volume, namely, the calcite aggregates volume and degree of coalescence, and the volume of the original matrix; (2) connected porosity: volume of interstitial and non-fabric-selective porosity; and (3) diagenetic constituents: types and volume of main diagenetic constituents affecting porosity, including both matrix replacement and filling matrix dissolution pores.

For reworked rocks, three petrofacies were defined: IntracDol, IntracSil, and IntracPor. To define petrofacies in intraclastic rocks, the following criteria were used: (1) total volume of connected porosity, corresponding to the sum of interparticle porosity and non-fabric-selective porosity (vugs, channels, and fracture pores); (2) main diagenetic constituent controlling porosity connection, which can be cementation by dolomite, silica, or calcite. In addition to in-situ and reworked rocks, one more reservoir petrofacies was defined for pervasively dolomitized crystalline rocks (DolostonePor).

The 13 defined petrofacies were grouped into four distinct petrofacies associations, classified as non-reservoir, poor, fair, good and very good (Fig. 11).

Geometry and distribution of porosity in the petrofacies

The pore space in pre-salt spherulitic reservoirs derives from the diagenetic dissolution of the original matrix composed by magnesian clays within which the calcite spherulites grew (Tosca and Wright 2015; Wright and Barnett 2015; Carramal et al., 2022). In contrast, in the shrubstones, porosity was developed both as primary, growth-framework pores among the calcite shrubs (Herlinger et al., 2023) and by the extensive dissolution of the inter-shrub matrix (Schrank et al., 2024). Porosity of the intraclastic rocks is more conventional, similar to typical carbonate and siliciclastic rocks (Herlinger et al., 2017; 2023), and is controlled by both depositional and diagenetic factors, as shown by Altenhofen et al. (2024). Particle size remains a fundamental control of their pore system, where coarser-grained particles tend to have larger pores, throats and permeability, while better sorting results in higher original porosity (Herlinger et al., 2023).

The quality of pre-salt reservoirs was also significantly influenced by dolomitization and silicification promoted by diagenetic or hydrothermal processes (Lima and De Ros, 2019), which have commonly decreased porosity and permeability due to the reduction of pore throats. Different forms of silicification and dolomitization of the pre-salt carbonates of the Campos and Santos Basin in Brazil and the Kwanza Basin in Angola have been linked to early and late burial diagenetic, and to hydrothermal processes (Saller et al., 2016; Teboul et al., 2017; Vieira de Luca et al., 2017; Lima and De Ros, 2019; Lima et al., 2020; Basso et al., 2023; Strugale et al., 2024).

The use of x-ray micro-computed tomography allowed the visualization and quantification of rock components and a realistic description of the geometry of the pore systems in 3-D (De Boever et al., 2012; Matheus et al., 2023) and integration of these data with the reservoir petrofacies defined through systematic petrography. In this section, the pore systems of each petrofacies are presented, with their most representative pore types and connection patterns, which directly affects their permeability.

Very good reservoir quality

High permeability values are associated with petrofacies ShrPor due to large pore throats connecting mostly primary growth-framework pores formed among the fascicular calcite aggregates during their precipitation as crusts on the sediment-water interface (Herlinger et al., 2017; Hosa et al., 2020). The pore network is heterogeneous and complex, controlled by the essentially vertical growth of the fascicular aggregates, and the distribution of pores and throats is controlled by the coalescence and relative location of the shrubs, as described by Herlinger et al. (2023). The most important pore types are the inter-aggregate and vuggy pores, which significantly contribute to increased porosity and permeability. Figure 12A shows a microtomographic image from the pore system of a representative sample of this petrofacies. The connection among pores is shown in Figure 12B, where macropores interconnect forming large fluid conduits. The pores with the highest number of connections are highlighted in red. MudShrPor rocks exhibit over 15% interstitial, non-fabric selective porosity, mainly from inter-shrub matrix dissolution, reaching 33%. High permeability results from well-connected pores controlled by large throats (Herlinger et al., 2017; Hosa et al., 2020). Secondary inter-aggregate and vuggy pores dominate. MudSphePor shows >15% macroporosity from matrix dissolution, forming smaller pores than shrubstones (Herlinger et al., 2023). Main porosity is secondary inter-aggregate pores, with rare vuggy and intra-aggregate pores. IntracPor, reworked rocks with >15% macroporosity, rank among the best reservoirs alongside ShrPor. The pore system is complex, well connected, and controlled by particle size, featuring interparticle, intraparticle, vuggy, and fracture pores that boost permeability.

Good reservoir quality

In MudShrDolPor petrofacies samples, dolomite is a main diagenetic constituent, both directly replacing the original matrix and cementing the matrix dissolution porosity. The volume of interstitial and non-fabric selective porosity reaches 13%. The most common pores are inter-aggregate and intercrystalline, resulting from matrix dissolution, with few vugular pores. The average pore size is smaller than in MudShrPor (Table 3), due to the dolomite crystals. Although there is a good range of porosity, permeability values are lower because dolomite reduced the connection among the pores, as shown in (Figure 12D, where it is possible to see more spaced pores and with fewer connections (Fig. 12E). DolostonePor has >50% dolomite replacement, erasing original textures but maintaining relatively high macroporosity. High permeability stems from well-connected intercrystalline pores (Tamoto et al., 2024). Some large pores may be fracturing artifacts. Intracrystalline porosity, important here, was undetectable by micro-CT.

Fair reservoir quality

The IntracDol samples have low petrographic macroporosity (<10%) due to abundant dolomite content in the interstitial spaces, both filling interparticle porosity and replacing clay matrix and peloids. Where porosity reduction is dominated by dolomite cementation, a strong impact on throat size relative to pore size is observed, as described by Herlinger et al. (2023). A microtomographic image of the resulting complex pore system is shown in Figure 12G, with scattered pores, with few connections among them (Fig. 12H). Some cases show good permeability values, despite the interparticle presence of dolomite. This occurs where dolomite cementation created a network of intercrystalline pores, partially enlarged by slight dolomite dissolution (De Boever et al., 2012). The MudShrDol has heterogeneous pore systems: dolomite creates flow barriers and reduces average pore size, even in shrub-dominated facies.

Poor and Non-Reservoir quality

The ShrSil petrofacies refers to shrubstones with a large volume of inter-aggregate silica, and low porosity and permeability. Silica in the inter-aggregate space also occurs filling inter-aggregate and non-fabric selective porosity, as well as replacing minor clay matrix. The extensive silica cementation, reduced the originally high porosity and permeability related to the shrubstone texture (Basso et al., 2023). Such silica-cemented rocks may constitute flow barriers. This is supported by some cases of silicified samples, whose petrophysical porosity ranges from 8% to 12%, but permeabilities are less than 1mD. The pore system presented in Figure 12J shows a region with some clustered pores, while most of the sample lacks any porosity. Figure 12K shows that the areas with macropores are poorly connected, due to the presence of silica.

In MudSpheDol dolomite is also the main diagenetic constituent, either directly replacing the original matrix or cementing the matrix dissolution porosity. These samples exhibit only up to 5% of interstitial and non-fabric selective macroporosity. The abundant formation of dolomite in the inter-spherulites spaces was favored by the release of Mg^{2+} from the meta-stable magnesian clays (Fournier et al., 2018; Schrank et al., 2024), creating pore systems with very low porosity and permeability. The pores are restricted to intra-aggregate pores and poorly-connected vugs, which do not effectively contribute to permeability.

The MudSpheMtx features >15% preserved matrix, with small, unconnected pores and very low permeability. Mudstone samples have <8% macroporosity, with magnesian clay matrix preserved or replaced by microcrystalline calcite, dolomite, or silica. Rare pores are small, yielding very low permeability, mainly from laminated matrix dissolution, IntracSil has <10% porosity filled by interstitial silica, often cementing moldic and intraparticle pores. Despite relatively high macroporosity, permeability is low due to poor pore connectivity (Fig. 12M and Fig. 12N).

Size and shapes of the pores from the petrofacies

The extraction of morphological pore attributes followed the same methodology used by Herlinger et al. (2022). Two attributes related to pore size were analyzed: Area 3D, which is the pore boundary area responsible for the exposed surface of the external voxels, and EqDiameter, which represents the diameter of a sphere with the same volume (Herlinger et al., 2022). Additionally, one attribute related to pore shape, ShapeVA3d, defined as sphericity (the closer to 1, the more equant the pore is), was calculated using AVIZO software. The analysis revealed significant differences between the petrofacies, which are closely related to reservoir quality. As expected, the attributes related to pore size showed that the petrofacies associated with very good reservoir quality have larger pores (Fig. 13; Table 5).

The ShrPor (porous shrubstone) petrofacies show the highest permeability values, largely due to the tridimensional intercalation of the calcite fascicular shrubs, forming larger and less equant pores, with wider throats than the other petrofacies (Fig. 14A). The interparticle pores of the IntracPor petrofacies are more equant, and could be schematically represented as tetrahedral or rhombohedral, connected by more or less lamellar throats, similarly to the shapes of typical intergranular pores of siliciclastic rocks (Fig. 14B). In contrast, pores generated by matrix dissolution tend to be smaller, and frequently below the resolution of the x-ray microtomography equipment. The larger pores generated by dissolution of the laminated Mg-clay matrix are commonly lamellar (Fig. 14C), although laterally discontinuous. The pore systems of petrofacies where dolomitization is a major diagenetic process are also characterized by smaller pore sizes. The presence of dolomite rhombs scattered (‘floating’) within the pores, typically generated by partial replacement of the matrix followed by its dissolution, created pore systems with smaller pore size and lower pore-to-throat size ratio, which is expected to decrease the residual oil saturation of those petrofacies (Herlinger et al., 2023). On the other hand, pore-lining dolomite cement reduced the inter-aggregate porosity, in the in situ rocks, and the interparticle pores in the intraclastic rocks.

The pore shape attributes are also closely linked to the petrofacies. The highest average ShapeVA3D values are found in petrofacies with the presence of dolomite (the closer to 1, the more equant the pores are). This is a characteristic attribute of the intercrystalline pores among the dolomite rhombs. Another petrofacies with a high value is *Mudstone*. In this petrofacies, the higher value may be related to the microtomographic scan resolution. Here, most pores are smaller than the resolution, and the few detected pores, appear as points that are considered spherical in the calculation. The IntracSil petrofacies also show high ShapeVA3D values due to the pore-lining cementation of a large portion of the interparticle pores by silica, leaving only the center of the originally larger pores uncemented.

CONCLUSIONS

The integration of petrographic and petrophysical data into the geological reservoir model requires a careful upscaling process that transforms microscopic and laboratory observations into representative model-scale properties. Detailed modeling of pore systems is essential for optimizing hydrocarbon exploration and production in the Santos Basin pre-salt, as it enables the identification of key controls on reservoir quality, prediction of the spatial distribution of porosity and permeability, and reduction of uncertainties in the characterization of producing zones. This enhanced understanding directly contributes to better exploratory target selection, completion strategy planning, and more efficient field development. The analysis of Aptian pre-salt samples from three wells of two fields from Santos Basin allowed various observations and inferences regarding the pore system, pore types, and porosity geometry in the different established petrofacies.

- Petrographic and x-ray microtomography analyses revealed the high complexity of the pore systems of the pre-salt Barra Velha Formation in the Santos Basin. The interaction of depositional and diagenetic processes resulted in inter-aggregate, intra-aggregate, interparticle, intraparticle, intercrystalline, vuggy, fracture, and channel pores.

- The integrated application of microtomographic, petrophysical and petrographic analysis allowed enhanced characterization of reservoir quality and porosity geometry.

- Systematic petrographic characterization defined 13 petrofacies and 5 petrofacies associations (nonreservoir, poor, fair, good, and very good).

- Petrofacies with high reservoir quality are characterized by large and well-connected pores and high porosity, while petrofacies with low quality have reduced porosity, and smaller pores with low connectivity, mainly due to the presence of preserved matrix, dolomite, and silica.

- The segmentation of porosity through x-ray computed microtomography allowed the visualization of the 3-D pore systems and the quantification of pore sizes and their connections. Microtomography showed excellent correlation with the classification of petrofacies and the petrofacies associations defined by petrography.

- Dolomitization and silicification had a significant impact on the permeability of the petrofacies. Petrofacies with abundant dolomite show lower permeability values due to reduced pore throat sizes. Petrofacies with silica exhibit low permeability values and small pores.

- A detailed understanding of pore systems and accurate characterization of petrofacies are essential for optimizing hydrocarbon exploration and production in the Santos Basin pre-salt, as they are critical for upscaling and feeding reservoir models to make them more realistic.

- Despite the advances, significant challenges remain in characterizing the Santos Basin pre-salt reservoirs. The application of digital rock technologies integrated with detailed petrography can improve the understanding of depositional and diagenetic controls on reservoir quality, considering the complexity of the pre-salt carbonate pore systems.

- The characterization of the evolution and the main controls on the porosity of both the in situ and reworked pre-salt rocks are essential for understanding their complex pore systems. Such knowledge shall contribute to optimize the hydrocarbon exploration and production of the main Santos Basin reservoirs, as of equivalent reservoirs in other South Atlantic basins.

ACKNOWLEDGMENTS

This paper is part of the Master’s degree research of the first author in the Postgraduate Program in Geosciences (PPGGeo) of the Federal University of Rio Grande do Sul (UFRGS). We also acknowledge the infrastructure and support from the Institute of Petroleum and Natural Resources (IPR) of the Pontifical Catholic University of Rio Grande do Sul (PUCRS). Furthermore, we also would like to thank the support of the Brazilian National Agency for Petroleum, Natural Gas and Biofuels (ANP) for funding through the R&D levy regulation, and for permitting access to well cores, samples and thin sections for analysis.

REFERENCES

Aguillar, J., J. T. F. Oste, M. M. Erthal, P. F. Dal' Bó, Á. Rodríguez-Berriguete, M. Mendes, and H. Claes, 2024, Depositional and diagenetic processes in travertines: A comprehensive examination of Tocomar basin lithotypes, Northwest Argentina. Journal of South American Earth Sciences, 142, 104960. https://doi.org/https://doi.org/10.1016/j.jsames.2024.104960

Altenhofen, S.D., A.G. Rodrigues, L. Borghi, and L.F. De Ros, 2024. Dynamic re-sedimentation of lacustrine carbonates in the Buzios Field, pre-salt section of Santos Basin, Brazil. *Journal of South American Earth Sciences,* 138, 104863, doi: 10.1016/j.jsames.2024.104863

ANP, 2025. Agência Nacional do Petróleo, Gás Natural e Biocombustíveis. Boletim da Produção de Petróleo e Gás Natural, Maio 2025 / Número 177, 30p. https://www.gov.br/anp/pt-br/centrais-de-conteudo/publicacoes/boletins-anp/boletins/arquivos-bmppgn/2025/maio.pdf

Baptista, R. J., A. E. Ferraz, C. Sombra, E. V. Santos Neto, R. Plawiak, C. L. L. Silva, A. L. Ferrari, N. Kumar, and L. A. P. Gamboa, 2023, The presalt Santos Basin, a super basin of the twenty-first century. Super Basin Issue AAPG Bull. 107 (8), 1369–1389. doi:10.1306/04042322048

Basso, M., J. P. P. Souza, B. C. Z. Honório, L. H. Melani, G. F. Chinelatto, A. M. P. Belila, and A.C. Vidal, 2022, Acoustic image log facies and well log petrophysical evaluation of the Barra Velha Formation carbonate reservoir from the Santos Basin, offshore Brazil. *Carbonates Evaporites* 37, 50. https://doi.org/10.1007/s13146-022-00791-4

Basso, M., G. F. Chinelatto, A. M. P. Belila, L. C. Mendes, J. P. P. Souza, D. Stefanelli, A. C. Vidal, and J. F. Bueno, 2023, Characterization of silicification and dissolution zones by integrating borehole image logs and core samples: a case study of a well from the Brazilian pre-salt. *Petroleum Geoscience*, 29, petgeo2022-044, 10.1144/petgeo2022-044

Blaich, O. A., J. I. Faleide, and F. Tsikalas, 2011, Crustal breakup and continent-ocean transition at South Atlantic conjugate margins. Journal of Geophysical Research, Solid Earth, v. 116 (1), 38.

Camargo, M. M., Chinelatto, G. F., Basso, M., and Vidal, A. C., 2022, Electrofacies definition and zonation of the Lower Cretaceous Barra Velha Formation carbonate reservoir in the pre-salt sequence of the Santos Basin, SE Brazil: Journal of Petroleum Geology, v. 45, no. 4, p. 439–460, doi:10.1111/jpg.12827.

Carramal, N.G., D. M. Oliveira, A. S. M. Cacela, M. A. A. Cuglieri, N. P. Rocha, S. M. Viana, S. L. V. Toledo, S. Pedrinha, and L. F. De Ros, 2022, Paleoenvironmental insights from the deposition and diagenesis of Aptian Pre-Salt magnesium silicates from the Lula Field, Santos Basin, Brazil. *J. Sediment. Res.*, *92*, 12–31.

Carvalho, M. D., and F. L. Fernandes, 2021, Pre-salt depositional system: Sedimentology, diagenesis, and reservoir quality of the Barra Velha Formation, as a result of the Santos Basin tectono-stratigraphic development: In M. R. Mello, P. O. Yilmaz, and B. J. Katz (eds.), The supergiant Lower Cretaceous pre-salt petroleum systems of the Santos Basin, Brazil: Tulsa, Oklahoma, AAPG and Brazilpetrostudies, AAPG Memoir 124, p. 121–154.

Carvalho, A. M. A., Y. Hamon, O. G. Souza Jr., N. G. Carramal, and N. Collard, 2022, Facies and diagenesis distribution in an Aptian pre-salt carbonate reservoir of the Santos Basin, offshore Brazil: A comprehensive quantitative approach: Marine and Petroleum Geology, v. 141, 105708. https://doi.org/10.1016/j.marpetgeo.2022.105708

Chaboureau, A. C., F. Guillocheau, C. Robin, S. Rohais, M. Moulin, and D. Aslanian, 2013, Paleogeographic evolution of the central segment of the South Atlantic during Early Cretaceous times: Paleotopographic and geodynamic implications. Tectonophysics, v. 604, p. 191–223.

Chafetz, H. S, and S. A. Guidry, 1999, Bacterial shrubs, crystal shrubs, and ray-crystal shrubs: bacterial vs. abiotic precipitation. Sedimentary Geology, 126(1-4), 57-74.

Choquette, P. W, and L. C. Pray, 1970 Geologic nomenclature and classification of porosity in sedimentary carbonates: AAPG Bulletin, v. 54, p. 207– 250.

De Boever E., C. Varloteaux, F. H. Nader, A. Foubert, S. B´ekri, S. Youssef, and E. Rosenberg, 2012, Quantification and prediction of the 3D pore network evolution in carbonate reservoir rocks. Oil & Gas Science and Technology – Revue d'IFP Energies nouvelles; 67(1):161–78. https://doi.org/10.2516/ogst/2011170.

Della Porta, G., 2015, Carbonate build-ups in lacustrine, hydrothermal and fluvial settings: comparing depositional geometry, fabric types and geochemical signature, in: Bosence, D.W.J., Gibbons, K.A., Le Heron, D.P., Morgan, W.A., Pritchard, T., Vining, B.A. (Eds.), Microbial Carbonates in Space and Time: Implications for Global Exploration and Production. Geol. Soc. London Spec. Publ. 418, 17-68.

De Ros, L. F., and K. Goldberg, 2007, Reservoir petrofacies: a tool for quality characterization and prediction: American Association of Petroleum Geologists, Annual Convention and Exhibition, Long Beach, California, 50055, p. 1–6.

De Ros, L. F., K. Goldberg, M. Abel, F. Victoreti, M. Mastella, and E. Castro, 2007, Advanced acquisition and management of petrographic information from reservoir rocks using the Petroledge(r) System. In Proceedings of the AAPG Annual Convention and Exhibition, Long Beach, CA, USA, 1–4.

De Ros, L. F., 2018, Genesis and evolution of Aptian pre-salt carbonate reservoirs in southeastern Brazilian margin (abs.): Brazilian Petroleum Conference, Rio de Janeiro, Brazil, June 19–21, 2018, 1p., doi:10.13140/RG.2.2. 12290.09922

De Ros, L.F., and D. M. Oliveira, 2023, An operational classification system for the South Atlantic pre-salt rocks. J. Sediment. Res., 93, 693–704.

Dickinson, J. A. D., 1966, Carbonate Identification and Genesis as Revealed by Staining. Journal of Sedimentary Petrology, 36, 491-505.

Farias, F., P. Szatmari, A. Bahniuk, and A. B. França, 2019, Evaporitic carbonates in the pre-salt of Santos Basin - genesis and tectonic implications. Marine and Petroleum Geology, v. 105, p. 251–272.

Fouke, B. W., J. D. Farmer, D. J. Des Marais, L. Pratt, N. C. Sturchio, P. C. Burns, and M. K. Discipulo, 2000, Depositional facies and aqueous-solid geochemistry of travertine-depositing hot springs (Angel Terrace, Mammoth Hot Springs, Yellowstone National Park, USA). Journal of Sedimentary Research, 70(3), 565- 585.

Fournier, F., M. Pellerin, Q. Villeneuve, T. Teillet, F. Hong, E. Poli, J. Borgomano, P. Léonide, and A. Hairabian, A., 2018, The equivalent pore aspect ratio as a tool for pore type prediction in carbonate reservoirs. *AAPG Bulletin*; 102 (7): 1343–1377. doi: https://doi.org/10.1306/10181717058

Freitas, V. A., R. M. Travassos, and M. B. Cardoso, 2019, Bacia de Santos. Sumário Geológico e Setores em Oferta, Agência Nacional do Petróleo, Gás Natural e Biocombustíveis, 16ª Rodada de Solicitações. 19pp.

Gomes, J. P., R. B. Bunevich, L. R. Tedeschi, M. E. Tucker, and F. F. Whitaker, 2020, Facies classification and patterns of lacustrine carbonate deposition of the Barra Velha Formation, Santos Basin, Brazilian Pre-salt: Marine and Petroleum Geology, v. 113, 104176. https://doi.org/10.1016/j.marpetgeo.2019.104176

Grotzinger, J. P., and A. H. Knoll, 1999, Stromatolites in Precambrian carbonates: evolutionary mileposts or environmental dipsticks?. Annual review of earth and planetary sciences, 27(1), 313-358.

Herlinger Jr., R., E. E. Zambonato, and L. F. De Ros, 2017, Influence of diagenesis on the quality of lower Cretaceous Pre-Salt lacustrine carbonate reservoirs from northern Campos Basin, offshore Brazil. Journal of Sedimentary Research, v. 87, p. 1285-1313.

Herlinger Jr., R., and A. C. Vidal, 2022, X-ray µCt extracted pore attributes to predict and understand Sor using ensemble learning techniques in the Barra Velha pre-salt carbonates, Santos Basin, Ofshore Brazil. J. Pet. Sci. Eng. https://doi.org/10.1016/j.petrol.2022.110282

Herlinger Jr., R., L. F. De Ros, R. Surmas, and A. C. Vidal, 2023, Residual oil saturation investigation in Barra Velha Formation reservoirs from the Santos Basin, offshore Brazil: a sedimentological approach. Sediment. Geol. 448 https://doi.org/10.1016/j. sedgeo.2023.106372.

Hosa, A., R. A. Wood, P. W. M. Corbett, R. S. de Souza, and E. Roemers, 2020, Modelling the impact of depositional and diagenetic processes on reservoir properties of the crystal-shrub limestones in the 'Pre-Salt' Barra Velha Formation, Santos Basin, Brazil. Mar. Petrol. Geol. 112, 104100.

Jones, B., and R. W. Renaut, 1994, Crystal fabrics and microbiota in large pisoliths from Laguna Pastos Grandes, Bolivia. Sedimentology 41, 1171–1202. https://doi.org/ 10.1111/j.1365-3091.1994.tb01448.x.

Kumar, N., and L.A.P. Gamboa, 1979, Evolution of the São Paulo Plateau (southeastern Brazilian margin) and implications for the early history of the South Atlantic. Geological Society of America Bull 90, 281–293. https://doi.org/10.1130/0016-7606(1979)90<281:EOTSPP>2.0.CO;2. GSA Bulletin (1979) 90 (3): 281–293.

Lentini, M. R., S. I. Fraser, H. S. Sumner, and R. J. Davies, 2010, Geodynamics of the central South Atlantic conjugate margins: implications for hydrocarbon potential. Petroleum Geoscience, v. 16, p. 217–229.

Lima, B. E. M., and L. F. De Ros, 2019, Deposition, diagenetic and hydrothermal processes in the Aptian Pre-Salt lacustrine carbonate reservoirs of the northern Campos Basin, offshore Brazil. Sedimentary Geology, 383, 55-81.

Lima, B. E. M., L. R. Tedeschi, A. L. S. Pestilho, R. V. Santos, J. C. Vazquez, J. V. P. Guzzo, and L. F. De Ros, 2020, Deep-burial hydrothermal alteration of the PreSalt carbonate reservoirs from northern Campos Basin, offshore Brazil: Evidence from petrography, fluid inclusions, Sr, C and O isotopes. Marine and Petroleum Geology, 113(2020), 104-143.

Lønøy, A., 2006, Making sense of carbonate pore systems: AAPG Bulletin, v. 90, p. 1381-1405.

Matheus, G. F., M. Basso, J. P. P. Souza, A. C. Vidal, 2023, Digital Rock Analysis Based on X-ray Computed Tomography of a Complex Pre-salt Carbonate Reservoir from the Santos Basin, SE Brazil. *Transp Porous Med* 150, 15–44. https://doi.org/10.1007/s11242-023-01986-6

Mazzullo, S.J., and G. V. Chilingarian, 1992, Diagenesis and Origin of Porosity. In: Chilingarian, G.V., Mazzullo, S.J., Rieke, H.H. (Eds.), Carbonate Reservoir Characterization: A Geologic-Engineering Analysis, Part I: Developments in Petroleum Science30. Elsevier, Amsterdam, pp. 199-270

Mohriak, W. U., 2003, Bacias sedimentares da margem continental Brasileira. Geologia, tectônica e recursos minerais do Brasil, 3, 87-165.

Mohriak, W. U., P. Szatmari, and S. Anjos, 2012, Salt: geology and tectonics of selected Brazilian basins in their global context. Geological Society, London, Special Publications, 363(1), 131-158.

Moreira, J. L. P., C. V. Madeira, J. A. Gil, and M. A. P. Machado, 2007, Bacia de Santos. Boletim de Geociências da Petrobras, v. 15, n. 2, p. 531-549.

Pentecost, A., 1990, The formation of travertine shrubs: mammoth hot springs, Wyoming. Geological Magazine 127 (2), 159–168.

Pereira, M. J., F. J. Feijó, 1994, Bacia de Santos. Boletim de Geociências da Petrobras, Rio de Janeiro, v. 8, n. 1, p. 219-234.

Rezende, M. F., S. N. Tonietto, and M. C. Pope, 2013, Three-dimensional pore connectivity evaluation in a Holocene and Jurassic microbialite buildup. AAPG Bulletin, 97(11), 2085–2101. DOI:10.1306/05141312171

Riding, R., 2008. Abiogenic, microbial and hybrid authigenic carbonate crusts: components of Precambrian stromatolites. Geologia Croatica, 61(2-3), 73-103.

Rodríguez-Berriguete, A., P. F. Dal'Bo, B. Valle, and L. Borghi, 2022, When distinction matters: carbonate shrubs from the aptian Barra Velha Formation of brasilian's presalt. Sediment. Geol. 440, 106236 https://doi.org/10.1016/j.sedgeo.2022.106236.

Saller, A., S. Rushton, L. Buambua, K. Inman, R. Mcneil, and J. A. D. Dickson, 2016, Pre-Salt stratigraphy and depositional systems in the Kwanza Basin, offshore Angola. AAPG Bull, 100, 1135–1164.

Schrank, A. B. S., T. Dos Santos, S. D. Altenhofen, W. Freitas, E. Cembrani, T. Haubert, F. Dalla Vecchia, R. Barili, A. G. Rodrigues, A. Maraschin, and L. F. De Ros, 2024, Interactions between Clays and Carbonates in the Aptian Pre-Salt Reservoirs of Santos Basin, Eastern Brazilian Margin. *Minerals*, *14*, 191. https://doi.org/10.3390/min14020191

Silva, M.D., M. E. B. Gomes, A. S. Mexias, M. Pozo, S. M. Drago, R. S. Célia, L. A. C. Silva, P. Netto, L. B. Gomes, C. C. Porcher, N. Dani, D. Driemeyer, C. W. D. Ramnani, and J. F. Santos, 2022, Mineralogical Study of Levels with Magnesian Clay Minerals in the Santos Basin, Aptian Pre-Salt Brazil. *Minerals*, *11*, 970.

Strugale, M., B. E. M. Lima, C. Day, J. Omma, J. Rushton, J. P. R. Olivito, J. Bouch, L. Robb, N. Roberts, and J. Cartwright, 2024, Diagenetic products, settings and evolution of the pre-salt succession in the Northern Campos Basin, Brazil. In: J. Garland, A.J. Barnett, T.P. Burchette, and V.P. Wright, (Eds.) Carbonate Reservoirs: Applying Current Knowledge to Future Energy Needs. Geological Society Special Publication 548, London., 35 pp. https://doi.org/10.1144/SP548-2023-93

Tamoto, H., A. L. S. Pestilho, and A. M. B. Rumbelsperger, 2024, Impacts of diagenetic processes on petrophysical characteristics of the Aptian presalt carbonates of the Santos Basin, Brazil. *AAPG Bulletin*; 108 (1): 75–105. doi: https://doi.org/10.1306/05302322046

Teboul, P. A., J. M. Kluska, N. C. M. Marty, M. Debure, C. Durlet, A. Virgone, and E. C. Gaucher, 2017, Volcanic rock alterations of the Kwanza Basin, offshore Angola - insights from an integrated petrological, geochemical, and numerical approach. Mar. Pet.Geol. 80, 394–411.

Terra, G. J. S., A. R. Spadini, A. B. França, C. L. Sombra, E. E. Zambonato, L. C. S. Juschaks, L. M. Arienti, M. M. Erthal, M. Blauth, M. P. Franco, N. S. Matsuda, N. G. C. Silva, P. A. Moretti Jr., R. S. F. D'Avila, R. S. Souza, S. N. Tonietto, S. M. C. Anjos, V. S. Campinho, W. R. Winter, 2010, Classificação de rochas carbonáticas aplicável às bacias sedimentares brasileiras. Boletim Geociências Petrobras, 18, 9-29.

Tosca, N. J., and V. P. Wright, 2015, Diagenetic pathways linked to labile Mg-clays in lacustrine carbonate reservoirs: a model for the origin of secondary porosity in the Cretaceous pre-salt Barra Velha Formation, offshore Brazil. Geological Society, London, Special Publications, 435(1), 33-46.

Vieira de Luca, P. H., H. Matias, J. Carballo, D. Sineva, G. A. Pimentel, J. Tritlla, M. Esteban, R. Loma, J. L. A. Alonso, L. P. Jiménez, M. Pontet, and P. B. Martinez, 2017, Breaking barriers and paradigms in presalt exploration: The Pão de Açúcar discovery (offshore Brazil). In: R.K. Merrill and C.A. Sternbach, (Eds.) Giant fields of the decade 2000–2010: AAPG Memoir 113, Tulsa, Okla., p. 177–194.

Wang, Q., M. Tan, C. Xiao, S. Wang, C. Han, and L. Zhang, 2022, Pore-scale electrical numerical simulation and new saturation model of fractured tight sandstone. *AAPG Bulletin*; 106 (7): 1479–1497. doi: https://doi.org/10.1306/04132220165

Warren, J. K., 2006, Evaporites: sediments, resources and hydrocarbons. Springer, Berlin, pp 455–566.

Weger R. J., G. P. Eberli, G. T. Baechle, J. L. Massaferro, and Y-F. Sun, 2009, Quantification of pore structure and its effect on sonic velocity and permeability in carbonates. AAPG Bull 93(10):1297–1317. https://doi.org/10.1306/05270909001

Wennberg, O. P., G. McQueen, P. H. Vieira de Luca, F. Lapponi, D. Hunt, A. S. Chandler, A. Waldum, G. N. Camargo, E. Castro, and L. Loures, 2021, Open fractures in pre-salt silicified carbonate reservoirs in block BM-C-33, the Outer Campos Basin, offshore Brazil. Petroleum Geoscience, v. 27 no. 4, 16 pp. https://doi.org/10.1144/petgeo2020-125

Worden, R. H., P. J. Armitage, A. R. Butcher, J. M. Churchill, A. E. Csoma, C. Hollis, R. H. Lander, J. E. Omma, 2018, Petroleum reservoir quality prediction: Overview and contrasting approaches from sandstone and carbonate communities. In *Geological Society Special Publication* (Vol. 435, pp. 1–31). Geological Society of London. https://doi.org/10.1144/SP435.21

Wright, V.P., and Barnett, A.J., 2015, An abiotic model for the development of textures in some South Atlantic early Cretaceous lacustrine carbonates: Geological Society Special Publication, v. 418, p. 209–219, doi:10.1144/SP418.3.

Wright, V. P., and A. J. Barnett, 2017, Critically Evaluating the Current Depositional Models for the Pre-Salt Barra Velha Formation, Offshore Brazil. Search and Discovery Article #51439, adapted from Keynote Address given at AAPG/SEG International Conference and Exhibition, London, England, October 15-18. AAPG Search and Discovery, Article, 51439.

Wright, V. P., and A. J. Barnett, 2020, The textural evolution and ghost matrices of the Cretaceous Barra Velha Formation carbonates from the Santos Basin, offshore Brazil. Facies, 66(1), 7.

Wright, V. P., 2022. The mantle, CO2 and the giant Aptian chemogenic lacustrine carbonate factory of the South Atlantic: Some carbonates are made, not born. Sedimentology, 69: 47-73. https://doi.org/10.1111/sed.12835

FIGURE CAPTIONS

Figure 1 – Location map of the Santos Basin, showing the Pre-Salt Polygon, with an area of 149,000 square kilometers, the studied fields (in yellow), and the wells (in red).

Figure 2 - Lower Cretaceous stratigraphic chart for the Santos Basin (modified from Moreira et al., 2007 and Wright and Barnett, 2015).

Figure 3 – Analytical workflow performed on the studied samples.

Figure 4 - Summary of the main in situ classes of the analyzed samples according to the classification of De Ros and Oliveira (2023).

Figure 5 - Summary of the main reworked classes of the analyzed samples according to the classification of De Ros and Oliveira (2023).

Figure 6 - Summary of the description of the cores with the distribution of porosity and permeability throughout them.

Figure 7 - Main primary components observed in the studied wells. (A) Muddy Spherulstone with irregular distribution of Mg-clay matrix and calcite spherulites. Crossed polarizers (XP). (B) Shrubstone formed by large fascicular aggregates with preferential vertical growth. (XP) (C) Mudstone with plane-parallel lamination. Uncrossed polarizers (//P). F) Massive calcarenite with interparticle porosity (blue). (//P).

Figure 8 - Main diagenetic components observed in the studied wells. (A) Detail of blocky calcite covering fascicular calcite (yellow arrow) in shrubstone. (//P). (B) Blocky calcite rim calcite covering intraclast. (//P). (C) Blocky dolomite filling interparticle porosity among calcite intraclasts (stained). (//P). (D) Detail of matrix being replaced by blocky dolomite. (//P). (E) Shrubstone constituted by large coalesced fascicular aggregates with inter-aggregate porosity filled by chalcedony. (XP). F) Microcrystalline quartz replacing calcite spherulites (yellow arrow). (XP).

Figure 9 - Main types of pores identified in the studied rocks. (A) Inter-aggregate. (yellow arrow) and vugular porosity with remnants of peloidal matrix (red arrow) in shrubstone. (//P). (B) Pores from shrinkage of the laminated clay matrix, partially replaced by blocky dolomite. (//P). (C) Vugular porosity, partially reduced by dolomite cementation. (//P). (D) Interparticle, intraparticle (red arrow) and vugular porosity (yellow arrow) in intraclastic rock. (//P). (E) Detail of intraparticle porosity due to intraclast dissolution in intraclastic calcarenite cemented by silica. (//P). F) Detail of intercrystalline (red arrow) and intracrystalline (yellow arrow) porosity in dolomite (//P).

Figure 10 - Log cross plots of porosity x permeability showing the values for the lithologic classes in the three studied wells.

Figure 11 - Microtomographic images of examples of reservoir petrofacies applied to *in situ* and redeposited pre-salt reservoirs. After coding the petrofacies, they are grouped into associations directly related to reservoir quality (non-reservoir, poor, fair, good, very good).

Figure 12 - Pore systems of the petrofacies segmented through high-resolution X-ray microtomography of petrofacies. (A) Pore system of a ShrPor, (B) corresponding pore connections and (C) equivalent thin section. (D) Pore system of a MudShrDolPor*,* (E) corresponding pore connections and (F) equivalent thin section. (G) Pore system of an IntracDol

petrofacies and (H) corresponding pore connections and (I) equivalent thin section. (J) Segmented pore system of a ShrSil petrofacies, (K) corresponding pore connections and (L) equivalent thin section. (M) Segmented pore system of an IntracSil petrofacies, (N) corresponding pore connections and (O) equivalent thin section.

Figure 13 - Distribution of the average area 3-D pore size in the defined petrofacies.

Figure 14 - Schematic representation of the main pore systems of the studied rocks. (A) Pore scheme of shrubstones, represented by tetrahedral pores. (B) Schematic of pores in intraclast rocks, represented by tetrahedra connected by lamellae. (C) Schematic pores of muddy shrubstones, represented by lamellae, interrupted by the presence of spherulites.

Short CVs

William da Silveira Freitas - William da Silveira Freitas received a B.Sc. degree in geology from the Federal University of Rio Grande do Sul and an M.Sc. degree in geosciences from the same university. He has extensive experience with x-ray computed microtomography applied to reservoir rocks, diagenesis of carbonate rocks, digital rock technology, the study of porous media, and experience with synchrotron light experiments on pre-salt rocks. He has participated in research and development projects focused on the development of genetic and diagenetic models integrating various techniques in the pre-salt rocks of the Barra Velha formation, Aptian of the Santos Basin.

Thisiane Dos Santos - Geologist graduated from the Federal University of Rio Grande do Sul (2011), specializing in petroleum geology (PRH-12/ANP/UFRGS). Holds a PhD from the University of Aberdeen (UK), where he studied the provenance of Upper Cretaceous siliciclastic turbidites (Rosario Formation, Mexico). Consolidated experience in the characterization of siliciclastic and carbonate reservoirs, petrography of sediments and rocks, geological surveying, and integrating and interpreting geochemical and petrophysical data. Participated in research and development projects focused on developing genetic and diagenetic models of carbonate rocks from the Aptian interval, associated with the petroleum system of the pre-salt of the South Atlantic.

Mariane Trombetta - Mariane C. Trombetta received her B.Sc. degree from the Federal University of Pampa and M.Sc. degree in geosciences from the Federal University of Rio Grande do Sul (UFRGS). She is currently a Ph.D. candidate at UFRGS and researcher at Petroleum and Natural Resources of PUCRS.

Sabrina Danni Altenhofen - Sabrina Danni Altenhofen is a geologist with a Ph.D. in geosciences from the Federal University of Rio Grande do Sul. Currently, she is a researcher at the Institute of Petroleum and Natural Resources (IPR-PUCRS). Has experience in petrographic characterization of siliciclastic and carbonate rocks. Currently specializes in pre-salt carbonate rocks, with a focus on reworked facies.

Argos Belmonte Silveira Schrank - Argos Belmonte Silveira Schrank is a geologist with an M.Sc. and PhD from UFRGS in siliciclastic and pre-salt rocks, utilizing detailed petrographic analysis with complementary techniques to create depositional and diagenetic models on studied deposits' evolution. His latest work was on the Barra Velha Formation of the Santos Basin in IPR at PUCRS with a focus on in situ rocks.

Guilherme Martinez - Guilherme A. Martinez holds an M.Sc. in geochemistry from UFRGS and is currently a Ph.D. candidate at the same institution. With almost two years of experience at the Institute of Petroleum and Natural Resources, he worked on a research and development project focused on reservoir characterization of Santos Basin pre-salt rocks.

Anderson Maraschin - Anderson J. Maraschin is a geologist with experience in siliciclastic petrography and geochronology with a Ph.D. from UFRGS. He is currently the head of the Isotopes and Geochronoloy Laboratorie at Pontifical Catholic University of Rio Grande do Sul, Porto Alegre, Brazil.

Felipe Dalla Vecchia - **Felipe Dalla Vecchia** is a professor and researcher at Pontifical Catholic University of Rio Grande do Sul - PUCRS. He has held the position of director of the Institute of Petroleum and Natural Resources of PUCRS (IPR) since November 2017. He is a member of the permanent staff of the Graduate Program in Materials Technology and Engineering (PGETEMA). He earned a Ph.D. and a master's in materials technology and engineering from the Pontifical Catholic University of Rio Grande do Sul, and an undergraduate degree in control and automation engineering from the same university. His area of expertise is materials engineering, developing new materials and technologies for CO2 capture and conversion. He also conducts research in wellbore integrity, focused on oil and gas industry, by evaluating the performance of well cements and steel corrosion under CO2 supercritical conditions. His other areas of interest include biofuels, biogas, hydrogen, direct air capture and geological carbon storage.

Amanda Goulart Rodrigues - Amanda G. Rodrigues is a sedimentary petrologist with experience in siliciclastic and carbonate rocks and their implications for hydrocarbon reservoirs, in addition to having technical expertise in higher education teaching. Since 2020, she has worked as an adjunct professor at the Federal University of Rio Grande do Sul (Brazil), advising undergraduate and graduate students in this specialty.

Luiz Fernando De Ros - Luiz Fernando De Ros worked 9 years with reservoir characterization in the exploration and at the Research Center of Petrobras, before joining UFRGS in 1990. After obtaining a PhD in mineralogy and petrology at the University of Uppsala, Sweden, he returned to UFRGS, where he has been teaching, supervising, and conducting research in many projects with exploration companies such as Petrobras, Shell, Chevron, and Statoil.

Rosalia Barili - Rosalia Barili has extensive experience in carbonate rock analysis and completed her Ph.D. applying petrographic, isotopic, and geochemical methods to investigate evidence of aragonitic seas in Cambrian samples. Currently, she leads research projects focused on pre-salt reservoir rocks and usage of salt caverns for carbon capture and storage.

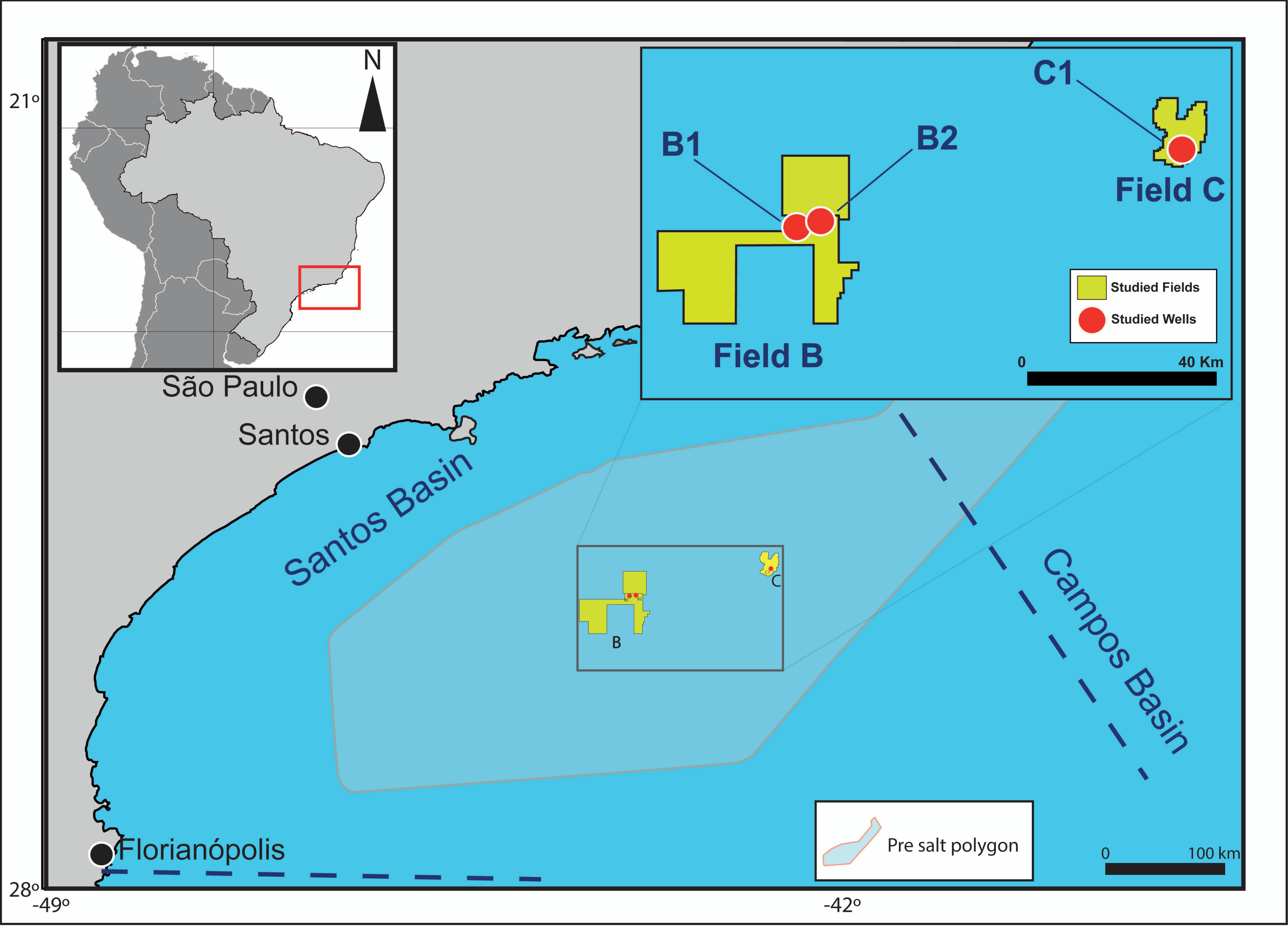
21º
28º
-49º
-42º
N
C1
B1
B2
Field C
Field B
Studied Fields
Studied Wells
0
40 Km
São Paulo
Santos
Santos Basin
C
B
Campos Basin
Pre salt polygon
0
100 km
Florianópolis

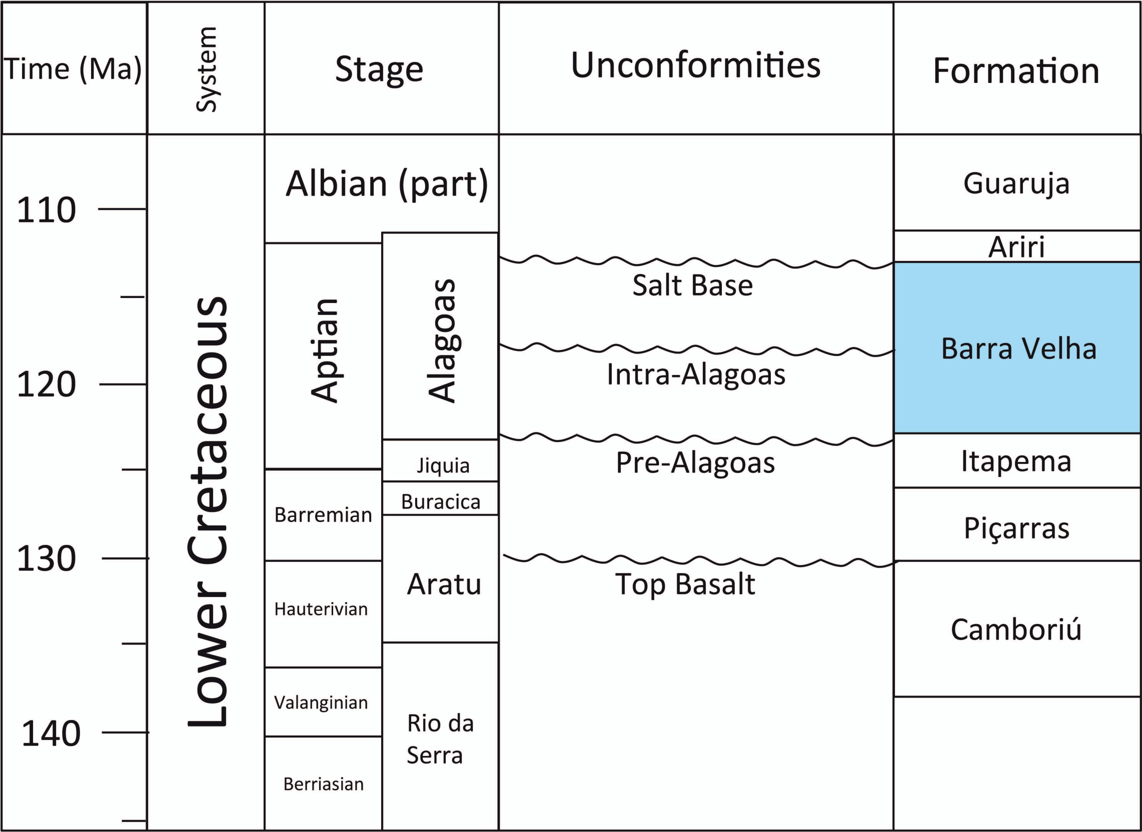
Time (Ma)
System
Stage
Unconformities
Formation
110
120
130
140
Lower Cretaceous
Albian (part)
Aptian
Barremian
Hauterivian
Valanginian
Berriasian
Alagoas
Jiquia
Buracica
Aratu
Rio da Serra
Salt Base
Intra-Alagoas
Pre-Alagoas
Top Basalt
Guaruja
Ariri
Barra Velha
Itapema
Piçarras
Camboriú

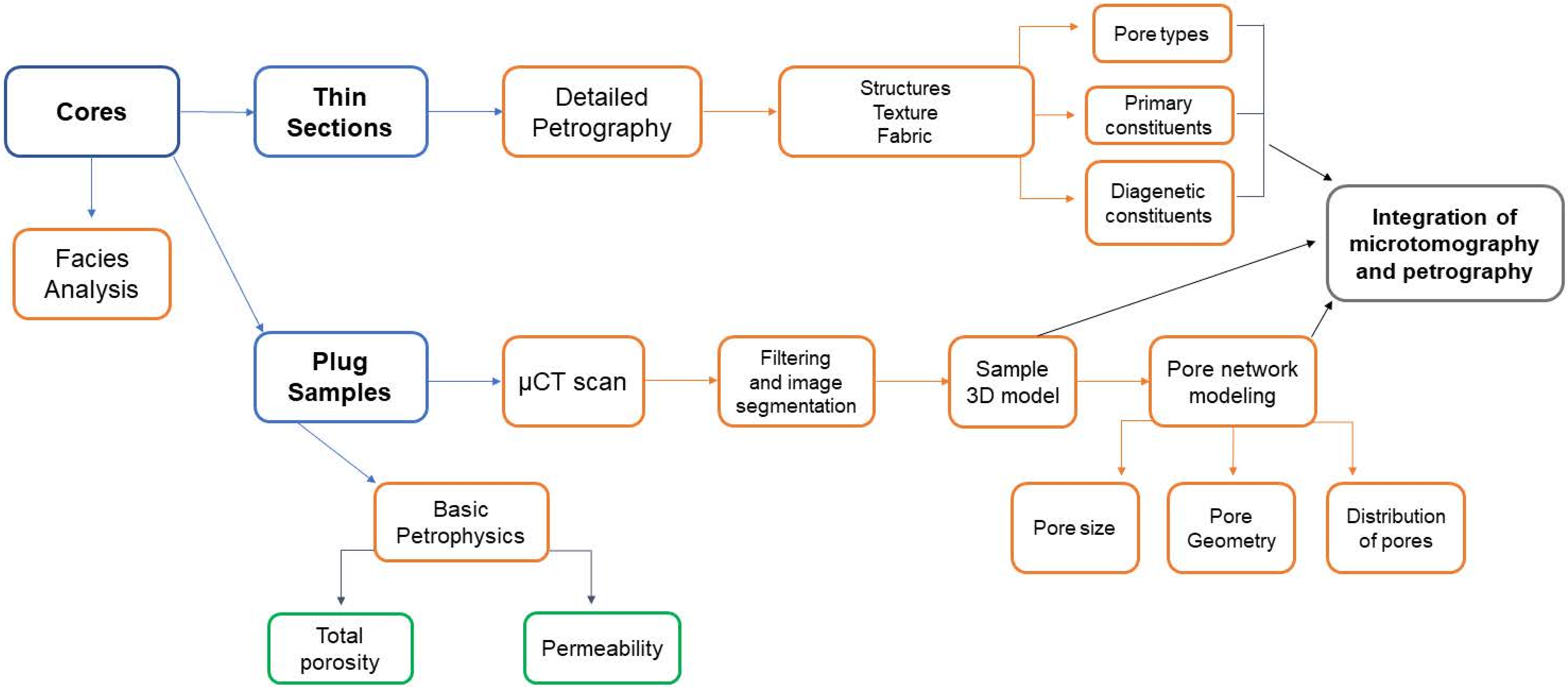
Cores
Thin Sections
Detailed Petrography
Structures
Texture
Fabric
Pore types
Primary constituents
Diagenetic constituents
Integration of microtomography and petrography
Facies Analysis
Plug Samples
µCT scan
Filtering and image segmentation
Sample 3D model
Pore network modeling
Pore size
Pore Geometry
Distribution of pores
Basic Petrophysics
Total porosity
Permeability

In situ

Sample	***Class***	***Description***
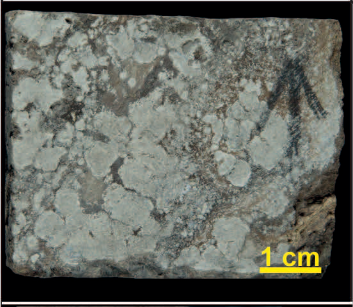	Muddy Shrubstones	Composed of shrubs and subordinate mud, usually with a massive texture. The shrubs are coalesced to partially coalesced; intra and inter-aggregate pores are common.
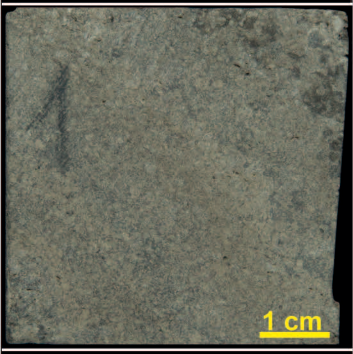	Shrubstones	Predominantly composed of shrubs and subordinate mud, generally of massive texture. The shrubs are coalesced to partially coalesced; intra- and inter-aggregate pores are common.
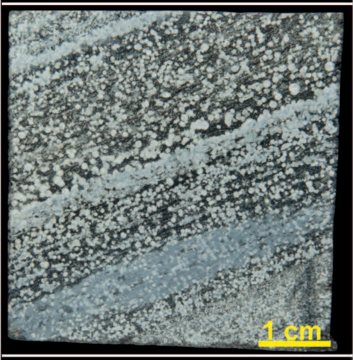	Muddy Spherulstones	Composed of non-coalesced spherulites, with significant amounts of mud, commonly exhibiting incipient to irregular or planar-parallel lamination.
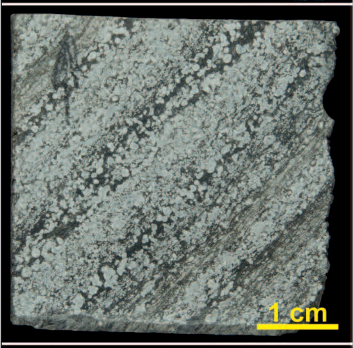	Spherulstones	Composed of coalesced spherulites, typically reaching a few millimeters in diameter. The spherulites are often silicified and dolomitized. Intra-aggregate, inter-aggregate, and vugular pores are common.
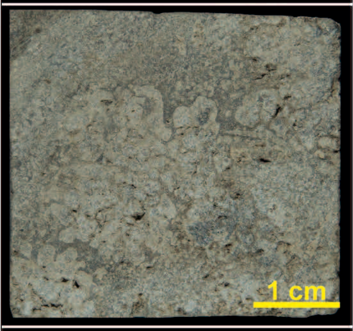	Shrub Spherulstones	Shrubs, spherulites, and mud dispersed or as laminations or transitional forms from one to another. Irregular to planar-parallel laminations often highlighted by dark mud or crusts of calcite aggregates.
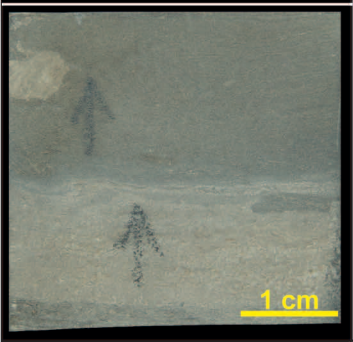	Mudstones	Millimetric to centimetric layers of mud, ranging from dark to white in color due to varying degrees of alteration. Incipient to irregular or planar-parallel lamination, sometimes deformed or displaced by silica.

Reworked

Sample	*Class*	*Description*
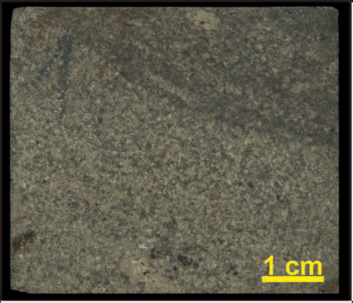	Calcarenites	Commonly massive or displaying planar-parallel lamination, moderately to poorly sorted, composed of millimetric to centimetric subrounded particles. The particles consist of fragments of calcite aggregates, mudstones, and chert. Interparticle and vugular pores are common.
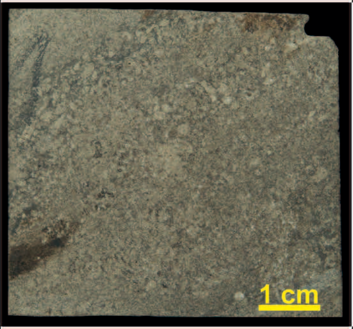	Rudaceous Calcarenites	Commonly massive or displaying irregular lamination, composed of moderately to poorly sorted, rounded particles up to 4 centimeters in size. Interparticle and vugular pores are common.
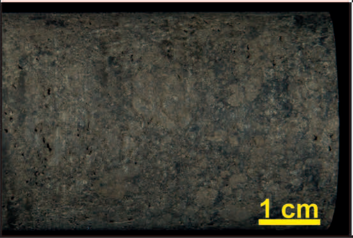	Calcirudites	Massive to irregularly laminated, coarse to very coarse poorly sorted, with angular to rounded particles. Vugular porosity is common.

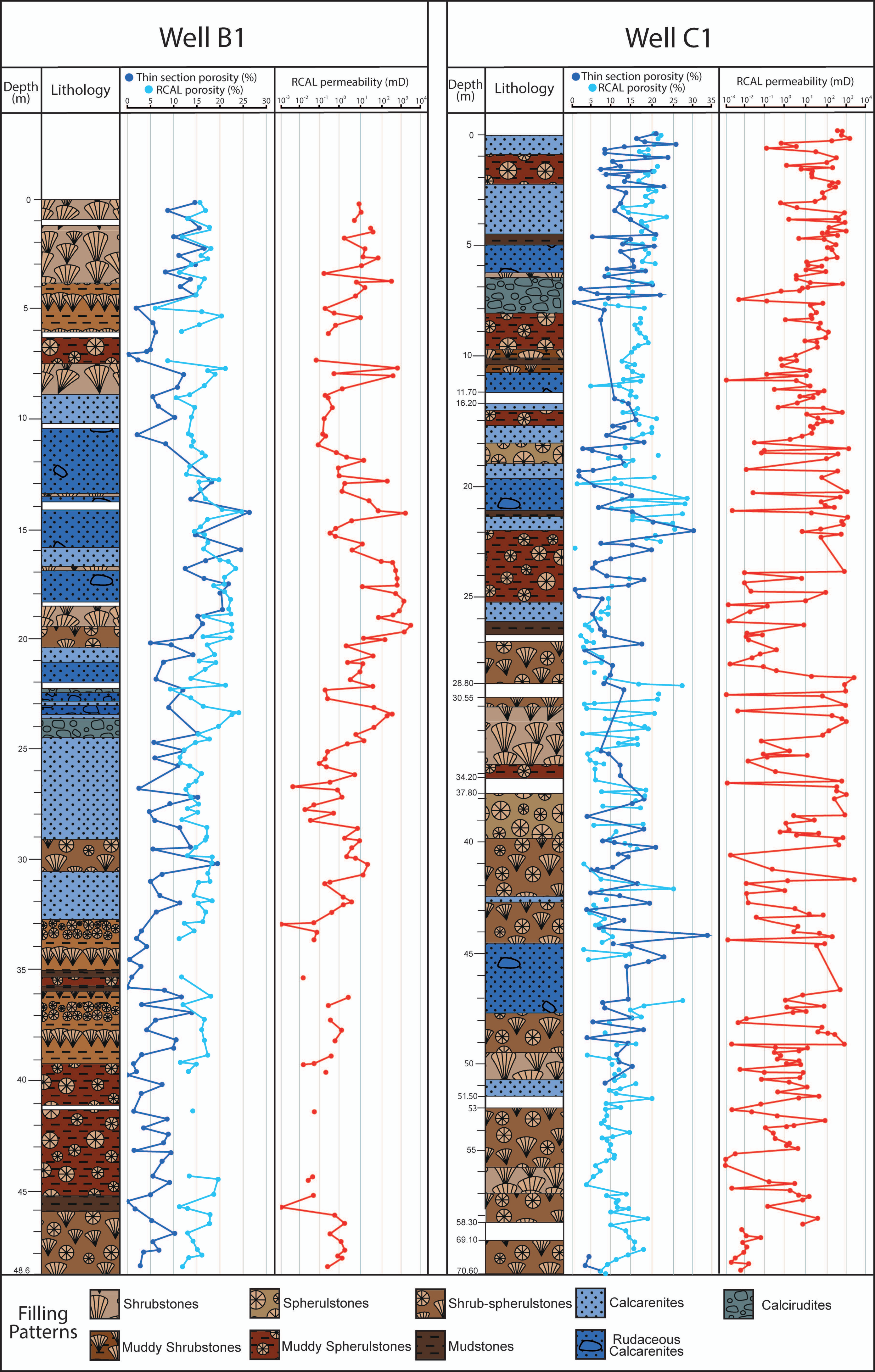
Well B1
Well C1
Depth (m)
Lithology
Thin section porosity (%)
RCAL porosity (%)
RCAL permeability (mD)
0 5 10 15 20 25 30
0 5 10 15 20 25 30 35
10⁻³ 10⁻² 10⁻¹ 10⁰ 10¹ 10² 10³ 10⁴
0
5
10
15
20
25
30
35
40
45
48.6
11.70
16.20
28.80
30.55
34.20
37.80
50
51.50
53
55
58.30
69.10
70.60
Filling Patterns
Shrubstones
Muddy Shrubstones
Spherulstones
Muddy Spherulstones
Shrub-spherulstones
Mudstones
Calcarenites
Rudaceous Calcarenites
Calcirudites

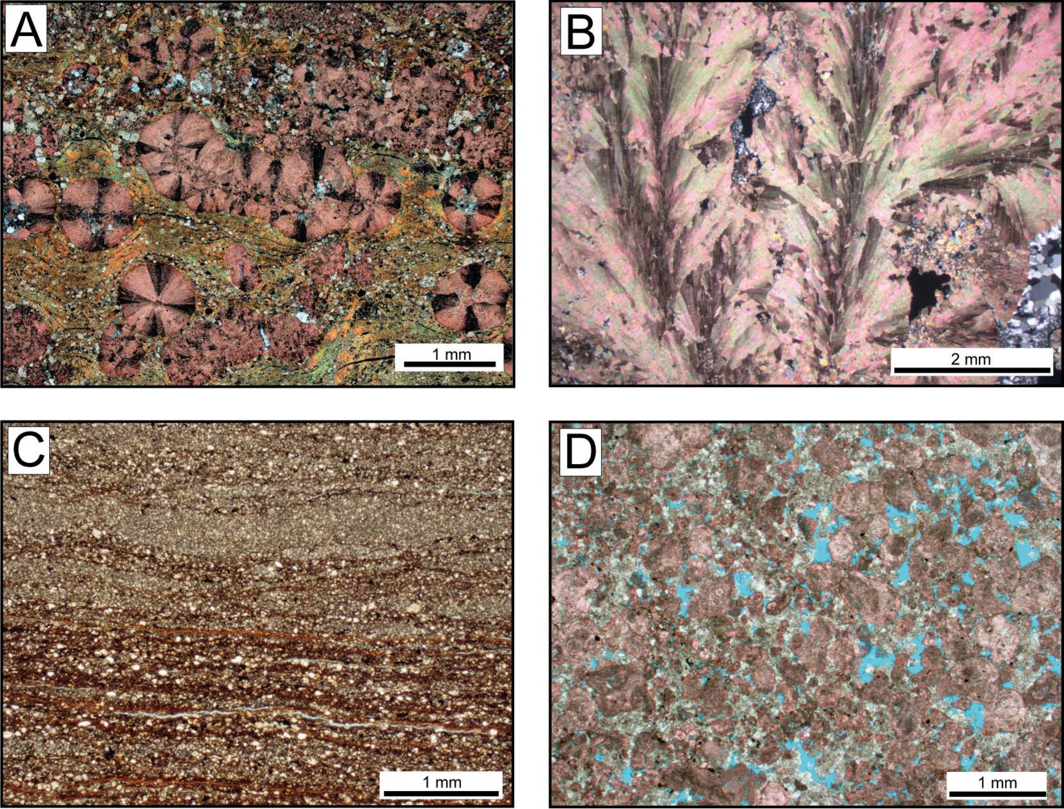
A
1 mm
B
2 mm
C
1 mm
D
1 mm

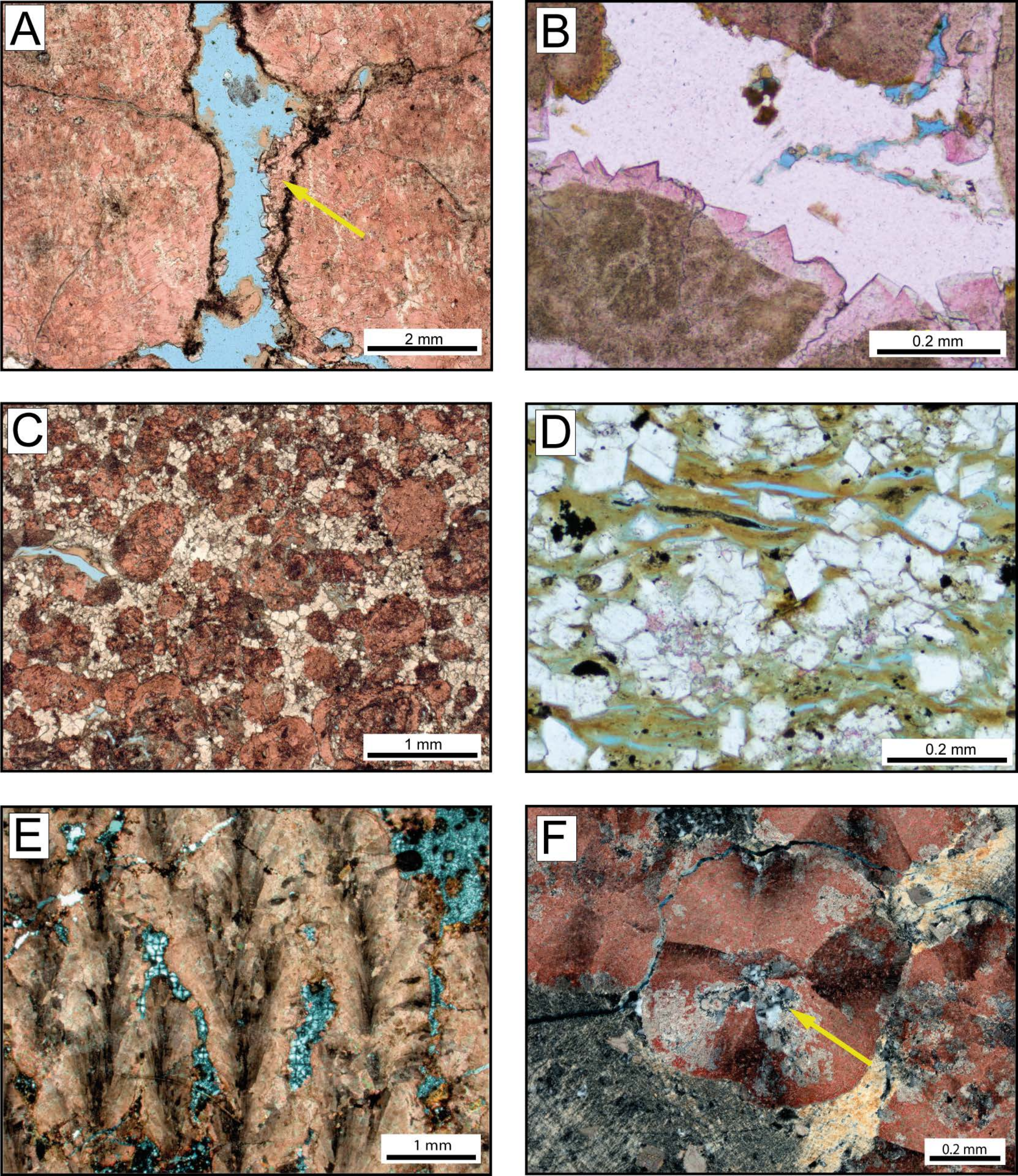
A
2 mm
B
0.2 mm
C
1 mm
D
0.2 mm
E
1 mm
F
0.2 mm

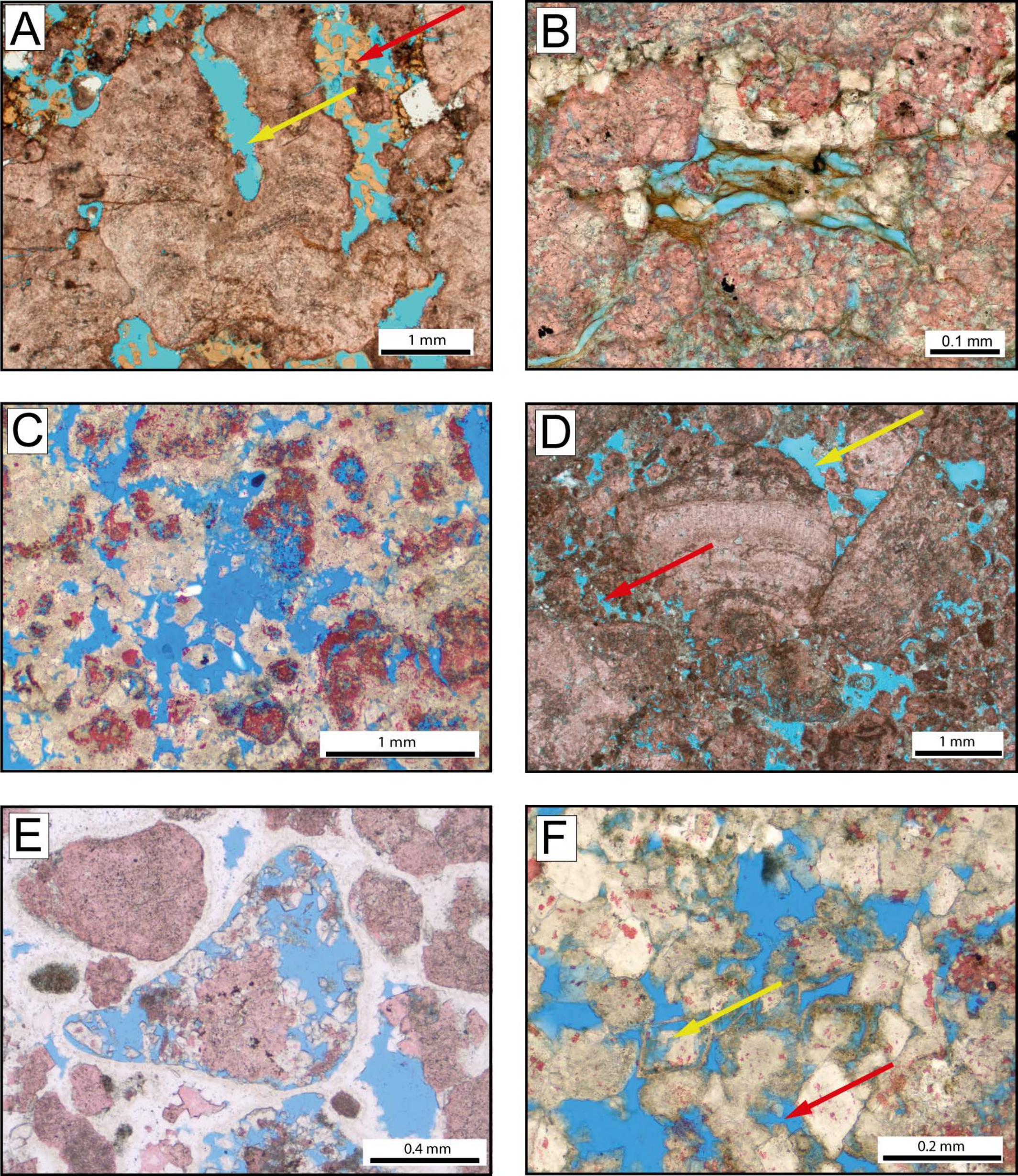
A
1 mm
B
0.1 mm
C
1 mm
D
1 mm
E
0.4 mm
F
0.2 mm

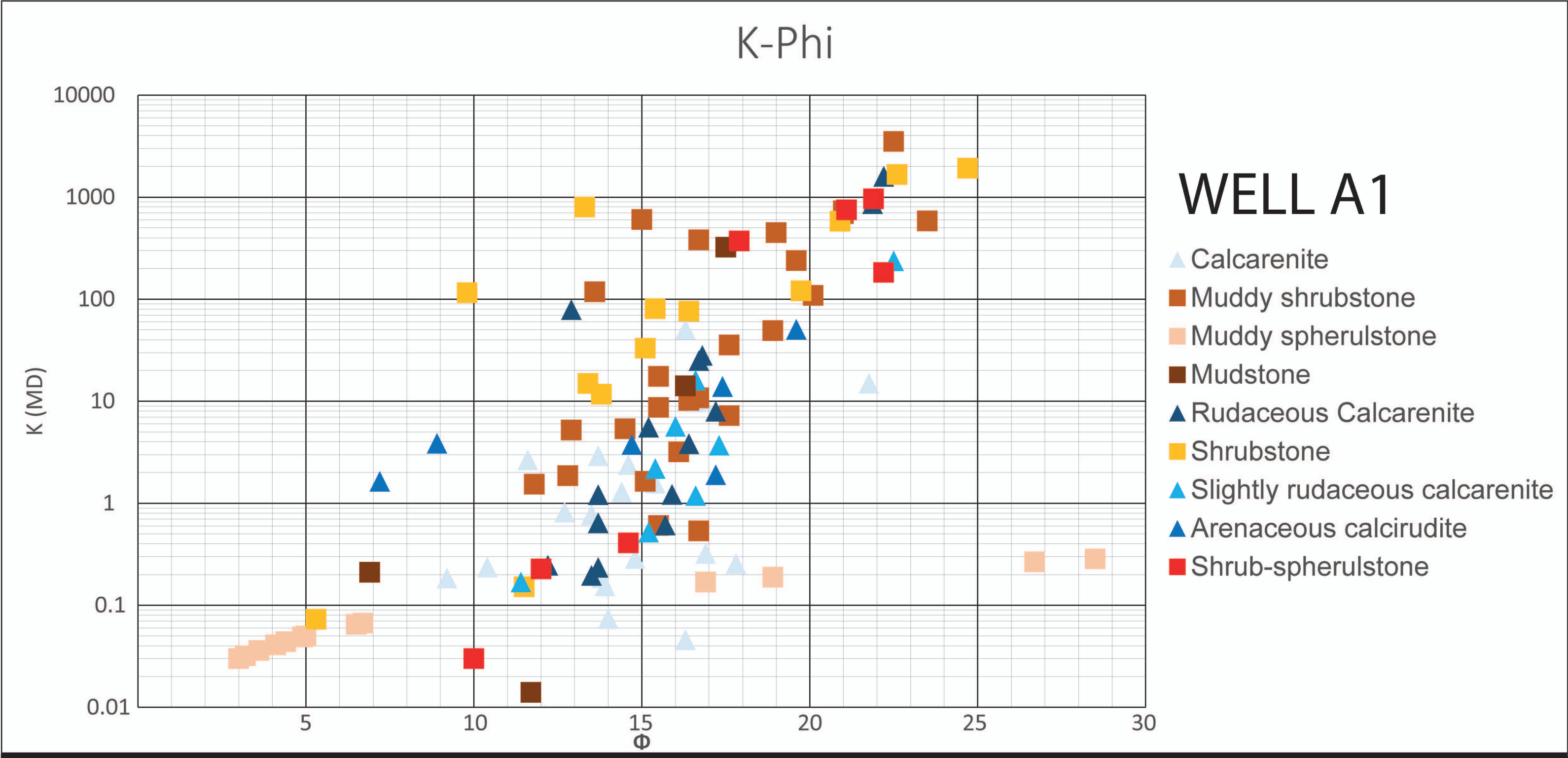
K-Phi
10000
1000
100
10
1
0.1
0.01
K (MD)
5
10
15
20
25
30
Φ
WELL A1
Calcarenite
Muddy shrubstone
Muddy spherulstone
Mudstone
Rudaceous Calcarenite
Shrubstone
Slightly rudaceous calcarenite
Arenaceous calcirudite
Shrub-spherulstone

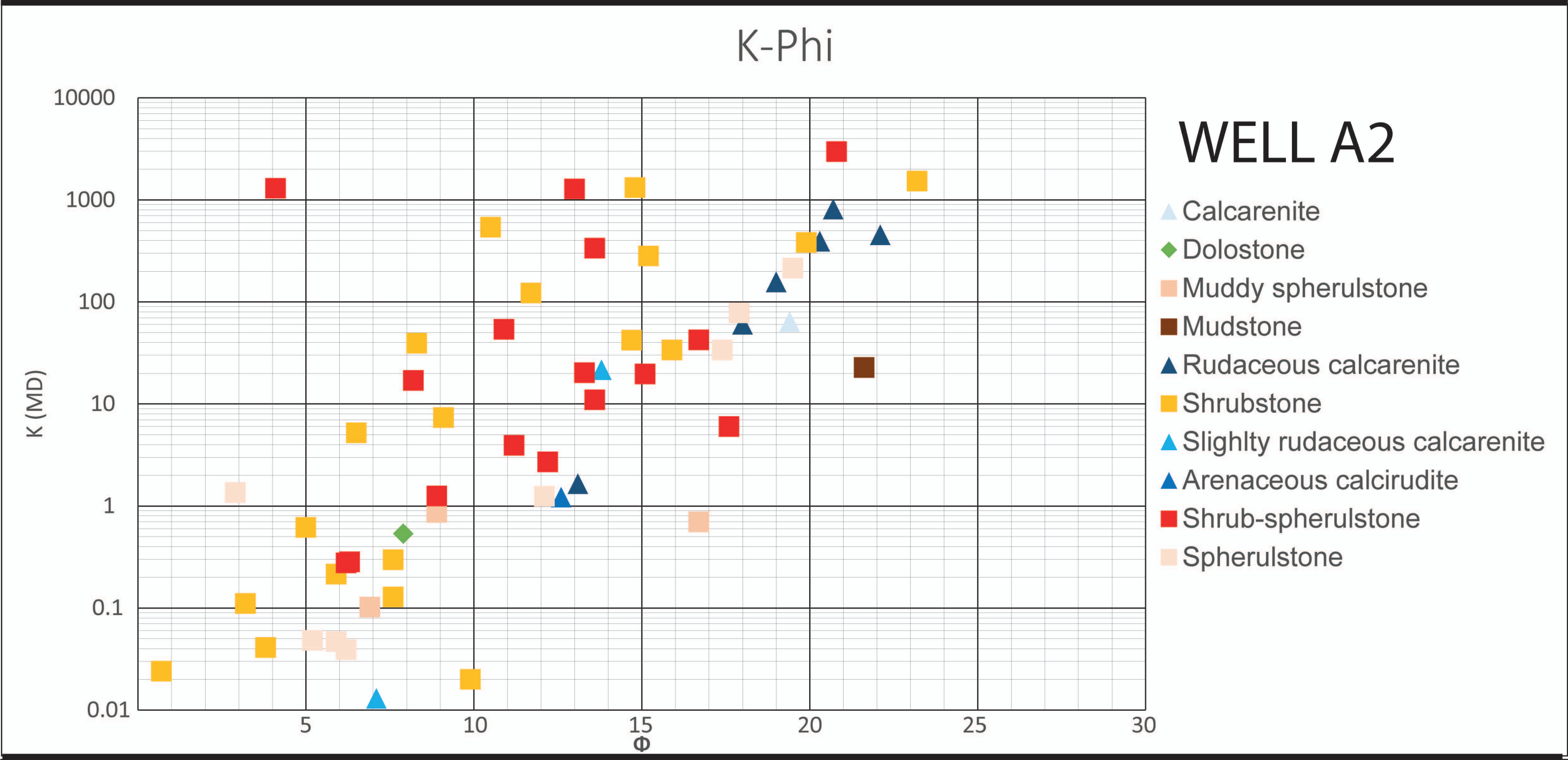
K-Phi
10000
1000
100
10
1
0.1
0.01
K (MD)
5
10
15
20
25
30
Φ
WELL A2
Calcarenite
Dolostone
Muddy spherulstone
Mudstone
Rudaceous calcarenite
Shrubstone
Slighlty rudaceous calcarenite
Arenaceous calcirudite
Shrub-spherulstone
Spherulstone

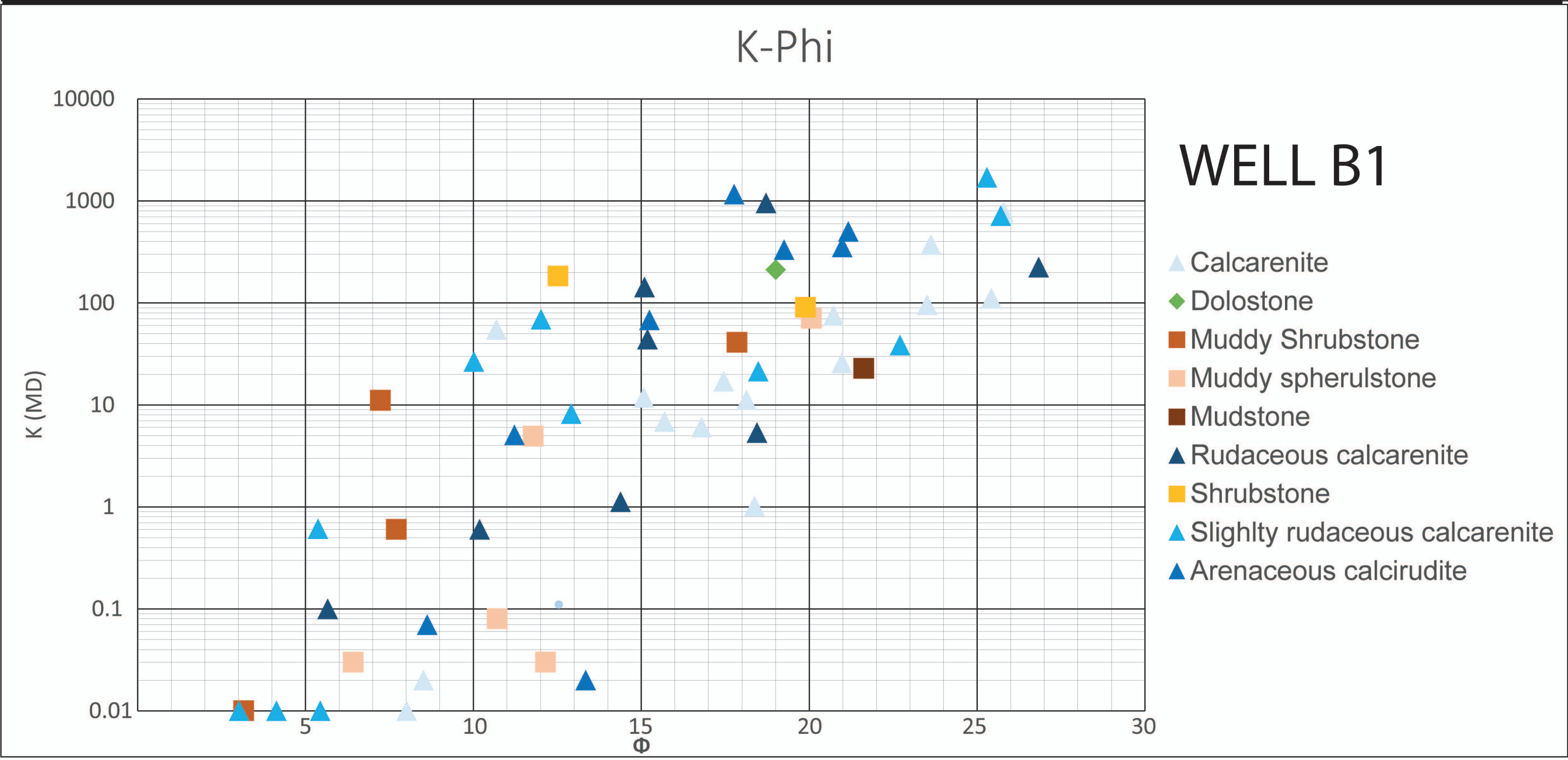
K-Phi
10000
1000
100
10
1
0.1
0.01
K (MD)
5
10
15
20
25
30
Φ
WELL B1
Calcarenite
Dolostone
Muddy Shrubstone
Muddy spherulstone
Mudstone
Rudaceous calcarenite
Shrubstone
Slighlty rudaceous calcarenite
Arenaceous calcirudite

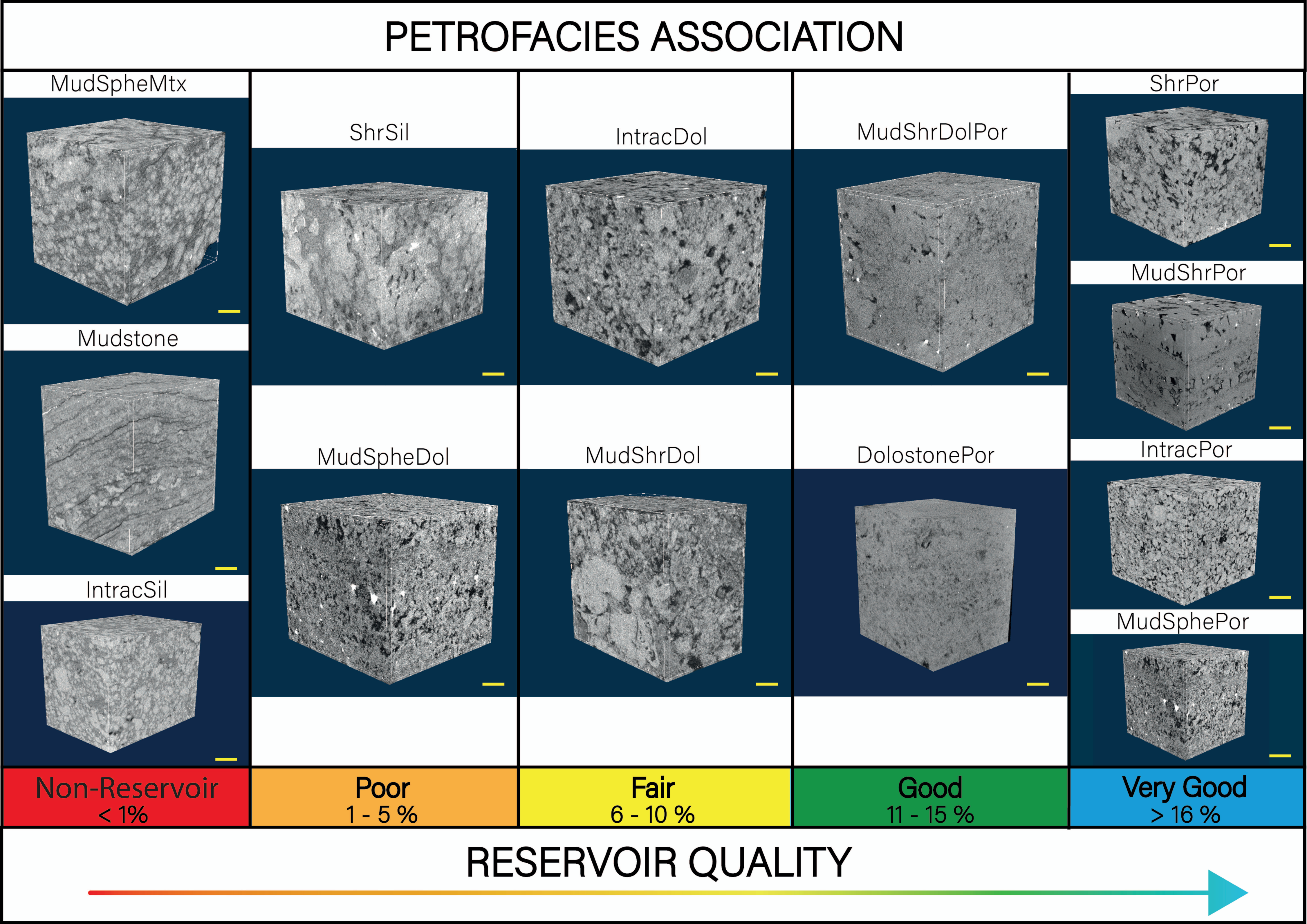
PETROFACIES ASSOCIATION
MudSpheMtx
Mudstone
IntracSil
ShrSil
MudSpheDol
IntracDol
MudShrDol
MudShrDolPor
DolostonePor
ShrPor
MudShrPor
IntracPor
MudSphePor
Non-Reservoir
< 1%
Poor
1 - 5 %
Fair
6 - 10 %
Good
11 - 15 %
Very Good
> 16 %
RESERVOIR QUALITY

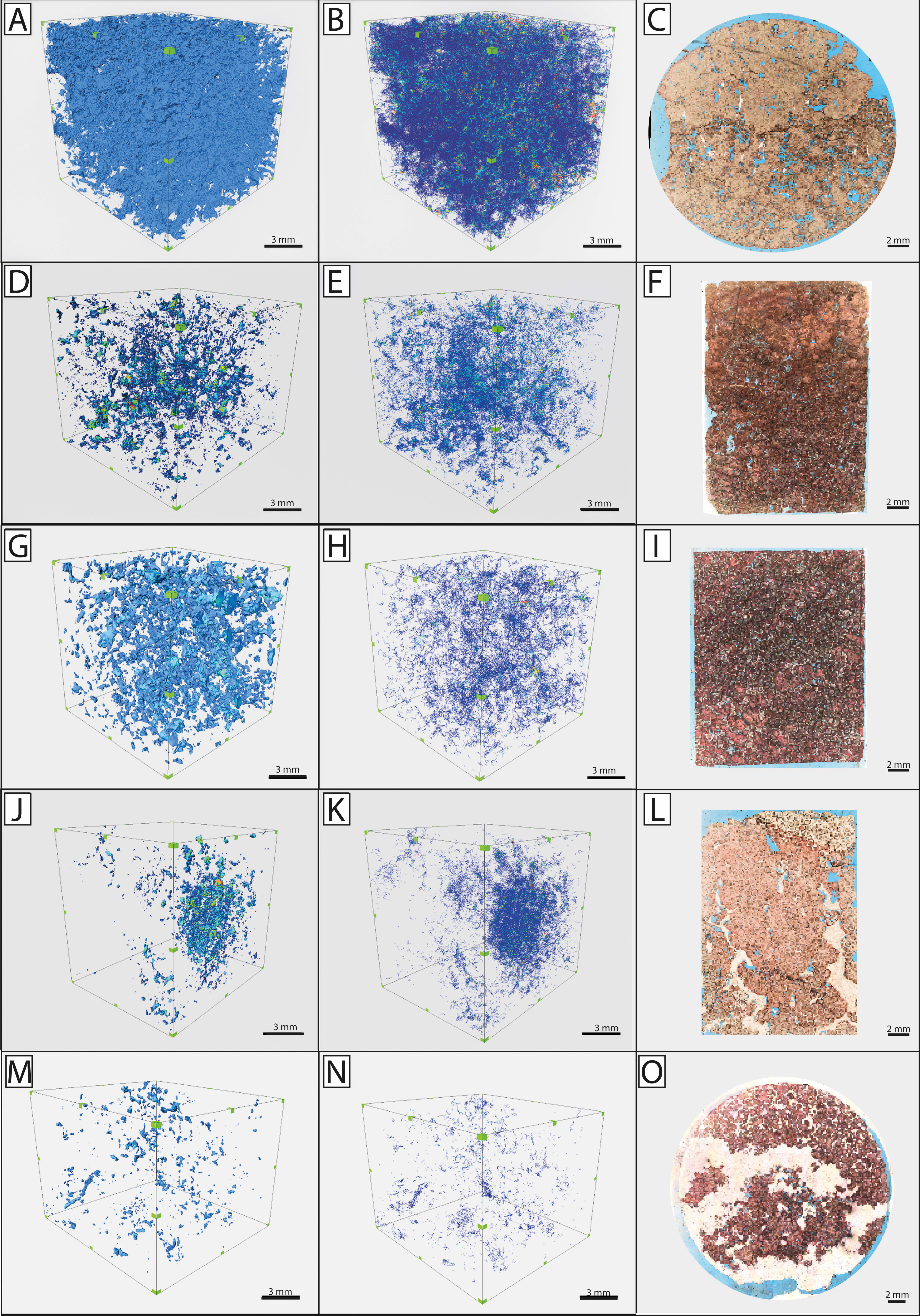
A
3 mm
B
3 mm
C
2 mm
D
3 mm
E
3 mm
F
2 mm
G
3 mm
H
3 mm
I
2 mm
J
3 mm
K
3 mm
L
2 mm
M
3 mm
N
3 mm
O
2 mm

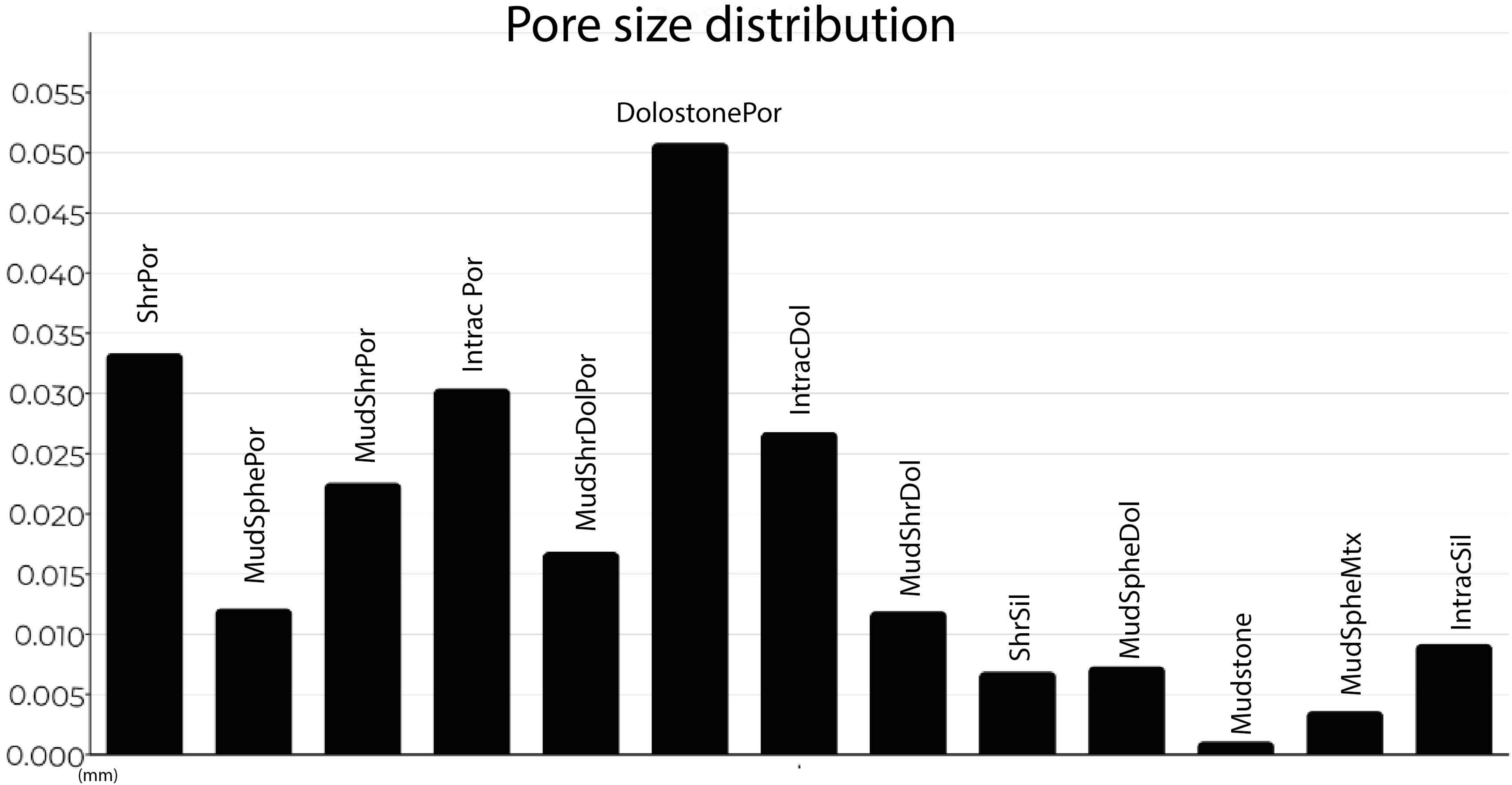

Pore size distribution

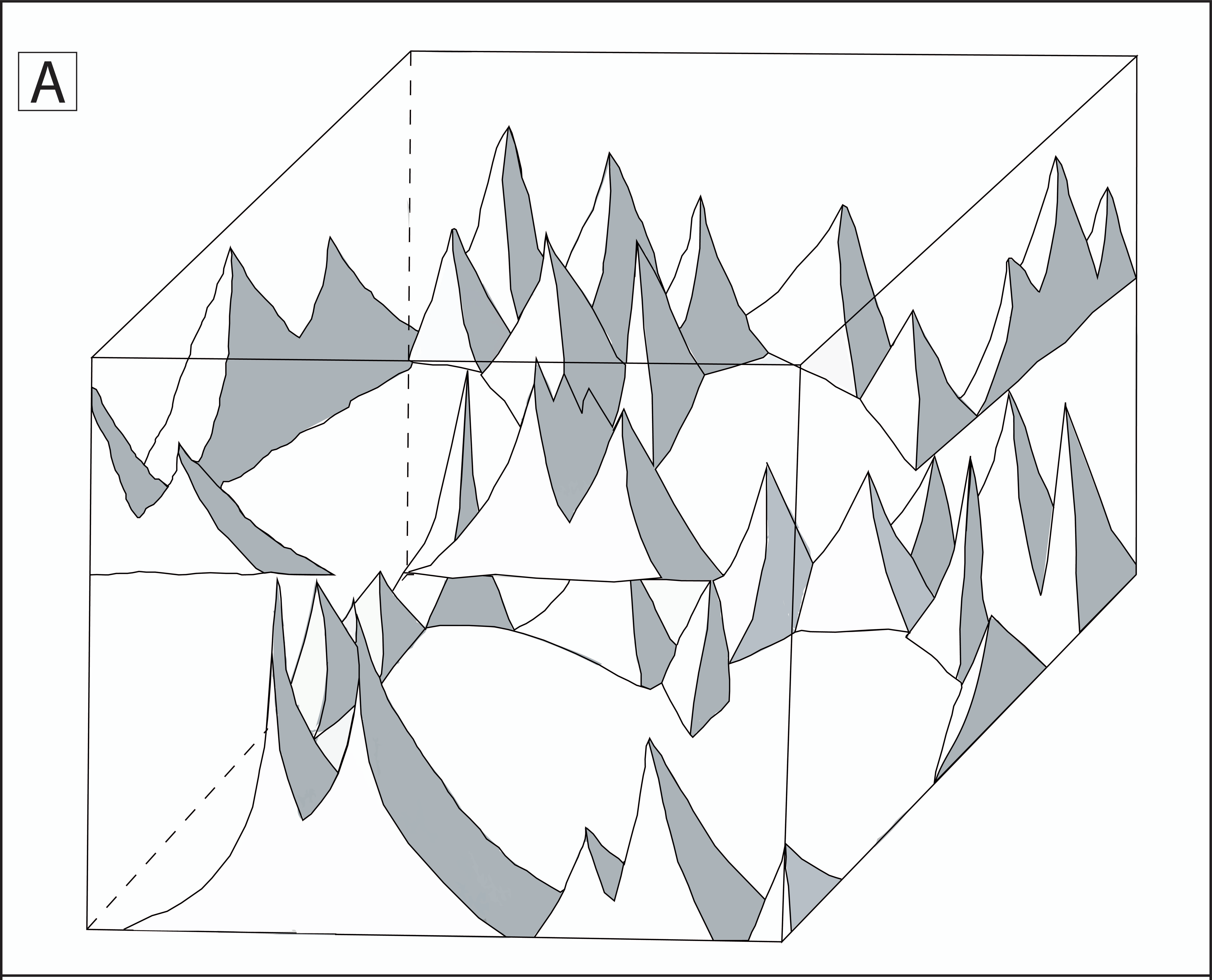
A

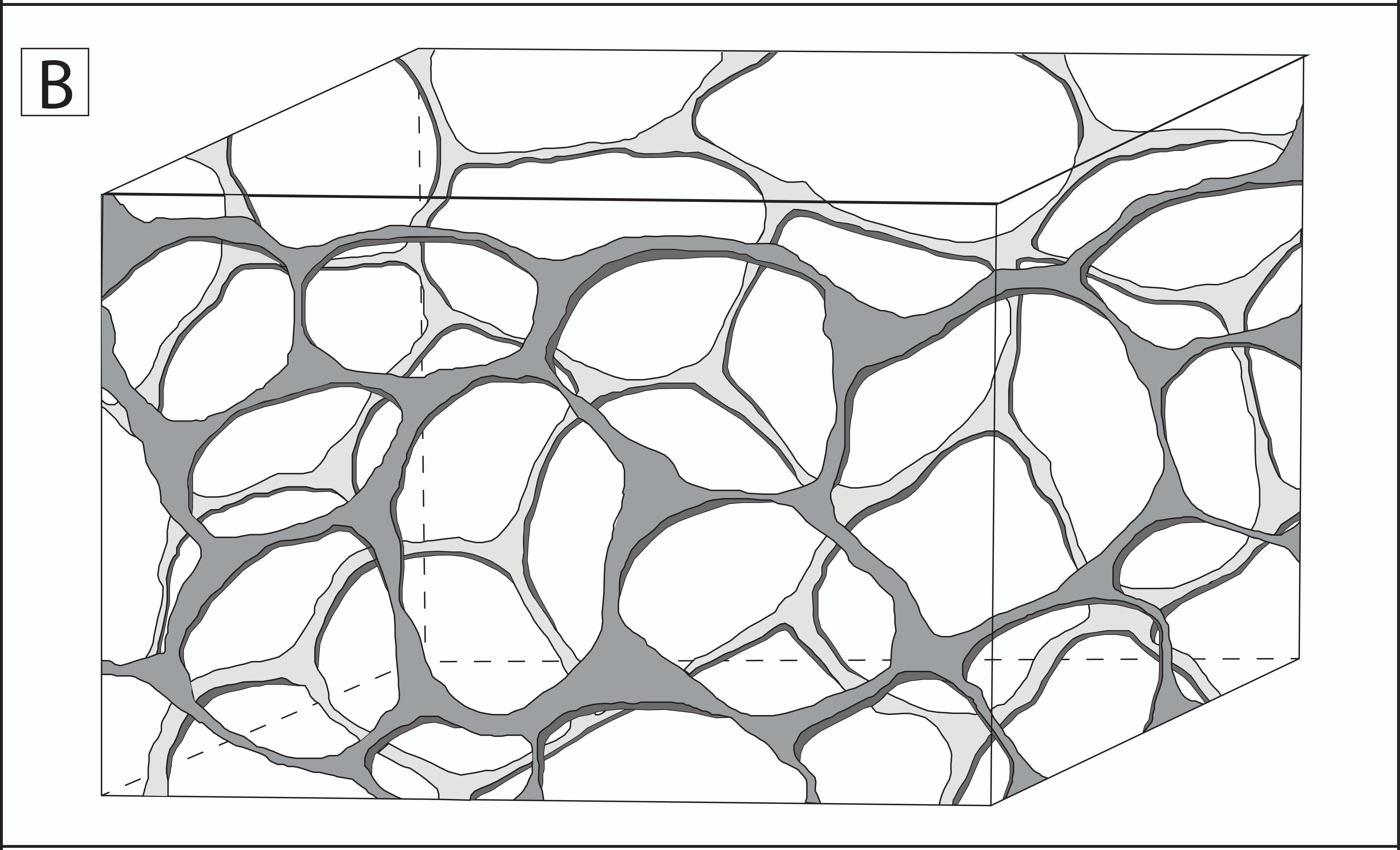
B

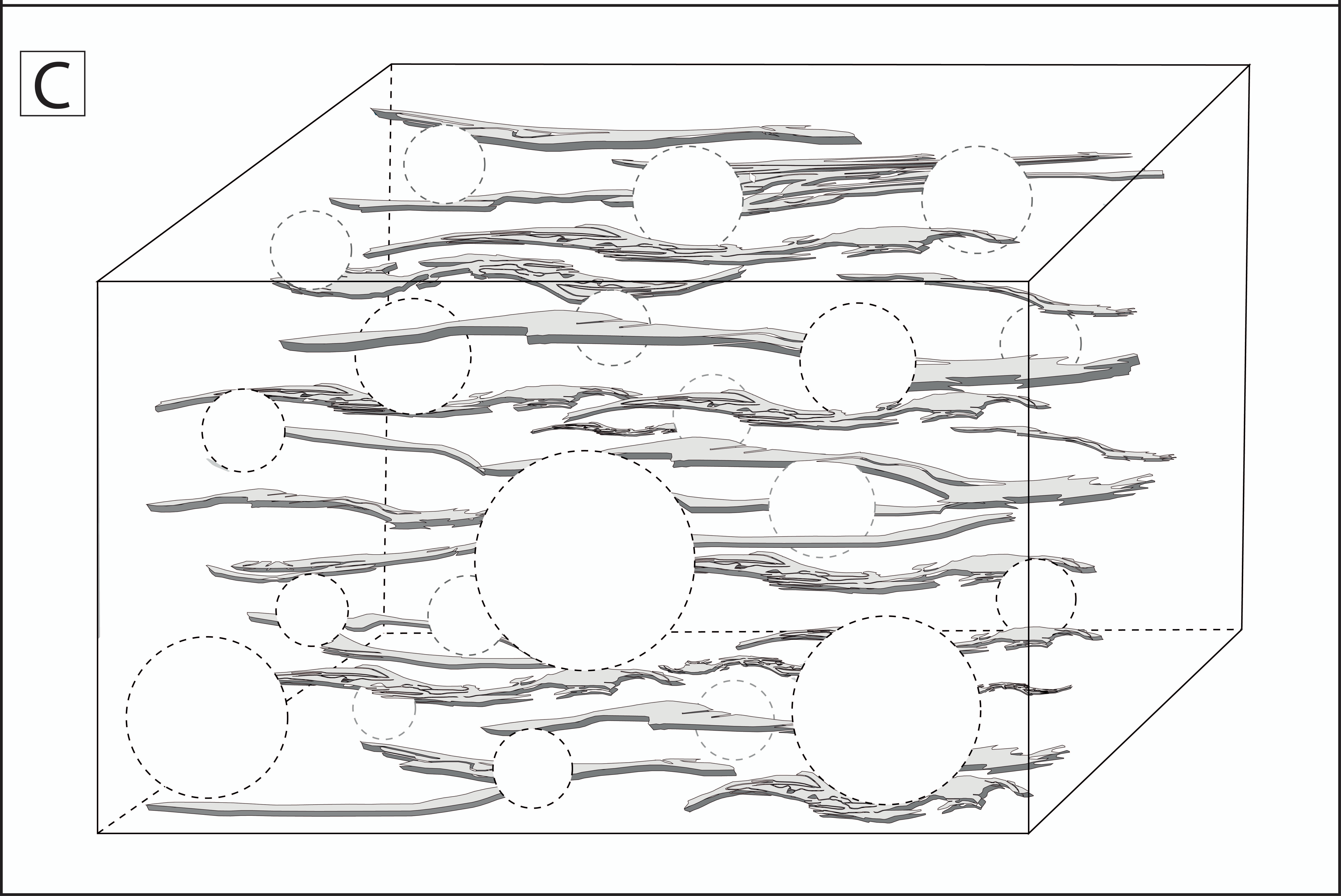
C

Table 1 - Maximum and average values of main original constituents.

Original composition Total	B1		B2		C1	
	Max. (%)	Avg. (%)	Max. (%)	Avg. (%)	Max. (%)	Avg. (%)
Spherulites	67.65	19.86	65.50	18.77	79.50	5.78
Shrubs	85.00	16.23	84.00	21.92	84.00	5.50
Matrix (laminated and peloidal)	97.50	32.60	100.00	31.83	100.00	16.66
Total Particles	77.50	22.06	75.50	9.29	89.50	41.33
Phosphate bioclasts	3.50	0.37	5.00	0.28	5.00	0.17
Mud intraclasts	1.33	0.01	0.50	0.00	7.00	0.19
Siliceous intraclasts	0.00	0.00	10.00	0.21	10.00	0.12
Carbonate intraclast	8.00	5.91	12.50	2.12	42.00	9.95
Other primary constituents	0.00	0.00	0.33	0.00	0.33	0.00
Detrital grains	13.00	1.41	6.00	0.58	6.00	0.20
Volcanic rock fragments	16.00	0.06	0.00	0.00	0.00	0.00

Table 2 - Maximum and average values of main diagenetic constituents.

Diagenetic Constituents	B1		B2		C1	
	Max. (%)	Avg. (%)	Max. (%)	Avg. (%)	Max. (%)	Avg. (%)
Total Calcite	**76.50**	**21.80**	**77.50**	**8.95**	**90.50**	**36.56**
Covering/Replacing Framework	25.00	0.08	2.00	0.27	5.00	0.12
Filling inter-aggregate/interparticle pores	26.00	0.28	7.33	0.13	31.00	0.56
Filling fabric non selective pores	7.33	0.79	2.00	0.03	32.00	0.86
Total Dolomite	**86.00**	**19.64**	**80.00**	**24.41**	**87.50**	**14.84**
Covering/Replacing Framework	84.00	1.26	60.00	1.61	80.50	1.72
Filling inter-aggregate/interparticle pores	40.50	1.45	48.00	1.47	48.00	1.46
Filling fabric non selective pores	14.67	0.31	8.00	0.29	12.00	0.81
Total Silica	**95.00**	**7.97**	**91.00**	**23.17**	**96.00**	**21.45**
Covering/Replacing Framework	11.00	0.11	64.00	1.63	64.00	2.53
Filling inter-aggregate/interparticle pores	36.00	1.11	50.00	1.64	69.50	1.90
Filling vugs, fractures and channels	22.00	0.47	74.00	4.14	74.00	4.55
Other diagenetic constituents	-	-	-	-	-	-
Sphalerite	0.00	0.00	4.00	0.03	4.00	0.00
Anhydrite	0.00	0.00	94.00	0.78	94.00	0.01
Barite	3.50	0.16	2.00	0.07	2.50	0.09
Dawsonite	1.67	0.02	0.00	0.00	2.00	0.04
Bitumen	8.15	0.18	16.00	0.88	16.00	0.19
Pyrite	9.00	1.21	5.00	0.94	5.50	0.42

Pre
Vers

Table 3 - Maximum and average values of pore types of *in situ* rocks.

Pore Types	B1		B2		C1	
	Max. (%)	Avg. (%)	Max. (%)	Avg. (%)	Max. (%)	Avg. (%)
Framework-Dissolution/Fracturing Pores	9.66	2.21	10.00	1.89	12.00	1.96
Matrix-Dissolution /Shrinkage/Inter-aggregate /Intercrystalline Pores	19.50	3.63	20.00	5.04	20.00	3.54
Interparticle Pores	0.00	0.00	1.50	0.02	1.50	0.01
Rock fracture Pores	2.00	0.12	3.00	0.23	3.00	0.26
Channel Pores	5.00	0.18	1.00	0.01	14.00	0.64
Vugular Pores	15.00	0.67	8.50	1.49	25.00	2.78

Table 4 - Maximum and average values of porosity types of reworked rocks.

Pore Types	B1		B2		C1	
	Max. (%)	Avg. (%)	Max. (%)	Avg. (%)	Max. (%)	Avg. (%)
Framework-Dissolution/Fracturing Pores	14.00	3.89	16.00	4.64	16.00	4.47
Matrix Dissolution/ Shrinkage/ Inter-aggregate/Intercrystalline Pores	15.00	2.87	4.00	0.22	12.00	0.97
Interparticle Pores	16.00	1.92	25.00	5.07	25.00	3.75
Rock fracture Pores	1.00	0.04	0.00	0.00	1.50	0.08
Channel Pores	2.67	0.10	0.67	0.04	0.67	0.10
Vugular Pores	5.00	0.63	7.00	2.59	20.00	2.88

Table 5 – Pore size and shape attributes of the reservoir petrofacies extracted from the microtomographic analyses.

PETROFACIES	PETROFACIES ASSOCIATION	*Pore Size Attribute*		*Pore shape attribute*
		Avg Area 3D	Avg EqDiameter	Avg ShapeVA3d
ShrPor	Very Good Reservoir Quality	0.033337	0.02962	0.00089
MudSphePor		0.012133	0.02898	0.00016
MudShrPor		0.022579	0.04081	0.00061
IntracPor		0.030390	0.02955	0.00066
MudShrDolPor	Good Reservoir Quality	0.016831	0.04230	0.88705
DolostonePor		0.050790	0.07787	0.98048
IntracDol	Fair Reservoir Quality	0.026802	0.03759	0.00045
MudShrDol		0.011911	0.03066	0.00013
ShrSil	Poor Reservoir Quality	0.006878	0.07793	0.00188
MudSpheDol		0.007327	0.03811	0.66146
Mudstone	Non-Reservoir	0.001086	0.03250	0.00012
MudSpheMtx		0.003619	0.02672	0.82055
IntracSil		0.009183	0.03220	0.97869

Prelimin
Version